Late Chromatoid Body and its Role in RNA Regulation During Spermatid Elongation

Master's Thesis

University of Turku

MSc Degree Programme in Biomedical Sciences

Drug Discovery and Development

May 2021

Salli Kärnä

Supervisors:

Mari Lehti, PhD

Noora Kotaja, PhD, Professor

Institute of Biomedicine

UNIVERSITY OF TURKU
Institute of Biomedicine, Faculty of Medicine

KÄRNÄ, SALLI: Late Chromatoid Body and its Role in RNA Regulation During Spermatid Elongation
Master's Thesis, 57 p
MSc Degree Programme in Biomedical Sciences/Drug Discovery and Development
May 2021

Spermatogenesis generates male gametes for reproduction. Spermiogenesis is the last part of spermatogenesis, where haploid male germ cells undergo differentiation from round spermatids to elongating spermatids and finally mature spermatozoa. During round spermatid differentiation, the chromatoid body (CB) functions as an RNA processing centre of the haploid male germ cells. In the beginning of spermatid elongation, the CB transforms into the late CB. Many of the RNA regulatory components get discarded, and other proteins start to accumulate to the late CB, such as testis-specific serine/threonine kinase 2 (TSSK2). The roles of TSSK2 and late CB in spermatogenesis remain largely unexplored. To investigate TSSK2 and late CB function, we co-immunoprecipitated TSSK2 interacting proteins and analyzed them with mass spectrometry. Eukaryotic initiation factor 3 (eIF3) complex was found as a novel interaction partner for TSSK2. Two hypotheses were formed: (i) TSSK2 and eIF3 interact in elongating spermatids, and (ii) the late CB has a role in the regulation of translation. The first hypothesis was tested with co-immunoprecipitation, immunofluorescence and proximity ligation assay, that all supported the nearby presence of TSSK2 and eIF3 in elongating spermatids and the late CB. The second hypothesis was tested with translational analysis, labelling newly synthetized proteins with L-azidohomoalanine. An accumulation of nascent proteins was detected in elongating spermatids in cytoplasmic sites corresponding to the late CB. In conclusion, this study reveals a novel interaction between TSSK2 and eIF3 in elongating spermatids and suggests that the late CB function is connected to translation and RNA regulation in male germ cells.

Key words: spermatogenesis, chromatoid body, late chromatoid body, TSSK2

Table of contents

1. Introduction

Spermatogenesis is the process that generates male gametes for reproduction and transmission of genetic material, ultimately ensuring the continuity and diversity of a species. The goal is to generate mature spermatozoa that are haploid, motile and able to reach and fertilize the female gamete, oocyte. This requires a complex programme of cell division and differentiation that takes place in the seminiferous tubules of the testis. Spermatogenesis can be divided into three functional phases: proliferation, meiosis, and postmeiotic germ cell differentiation known as spermiogenesis. The proliferation phase includes unsymmetrical mitotic cell divisions of the germline stem cells that both maintain the stem cell reserve and produce spermatogonia that initiate differentiation. In the next phase, spermatocytes divide twice in meiosis I and meiosis II to produce haploid spermatids. In the final phase of spermiogenesis, the haploid germ cells undergo multiple steps of differentiation from round to elongating spermatids, and finally, spermatozoa. The whole developmental programme takes several weeks to complete, occurring in repeating cycles in the seminiferous epithelium (Figure 1). (Russell et al., 1993; Hermo et al., 2010a)

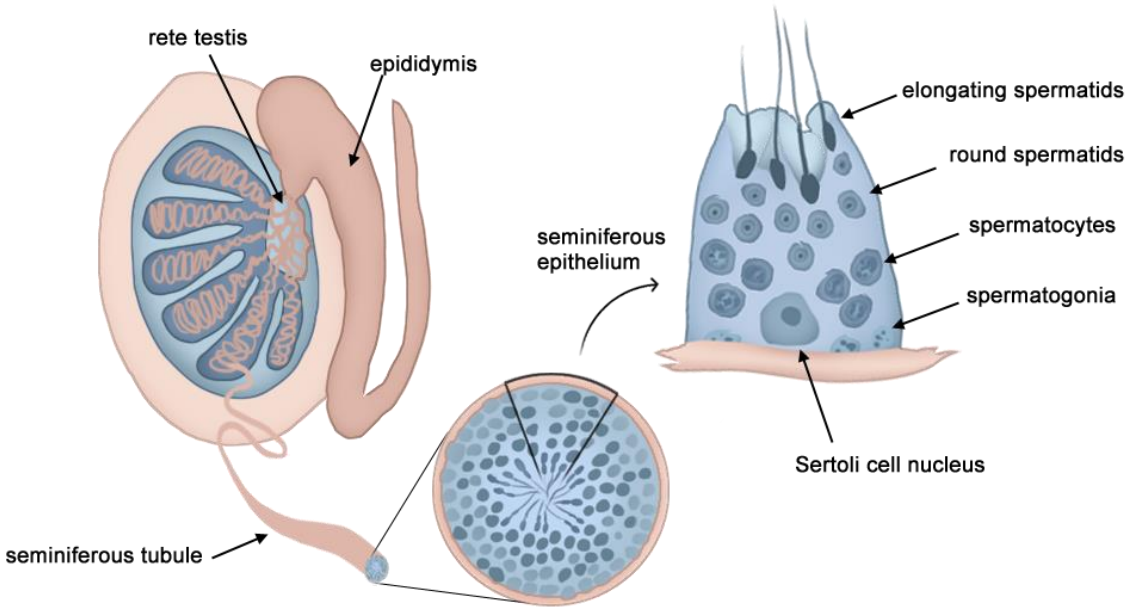

Figure 1. Organization of the testis and seminiferous tubules. Spermatogenesis takes place in the seminiferous tubules of the testis. The seminiferous tubules are looped inside the lobules of the testis and meet in rete testis, which connects the tubules to the epididymis via efferent duct. Inside the seminiferous tubule, seminiferous epithelium consists of layers of germ cells in different stages of differentiation. The germ cells are supported by the somatic pyramid-shaped Sertoli cells.

Each cross section of the seminiferous epithelium reveals a specific temporal stage of the seminiferous epithelial cycle, where a set of germ cells in different developmental phases are present and supported by somatic Sertoli cells. There are 6 such stages in human spermatogenesis and 12 in mouse spermatogenesis. In each stage, there is a strict organization of germ cells in the epithelium from its base to the tubular lumen. Spermatogonia reside in the layer at the base of the epithelium, spermatocytes occupy the next layer closer to the tubule lumen and spermatids reside on top, adjacent to the lumen. Mouse spermatogenesis and the different associated cell types of each stage are illustrated in the Figure 2. (Russell et al., 1993; Hermo et al., 2010a)

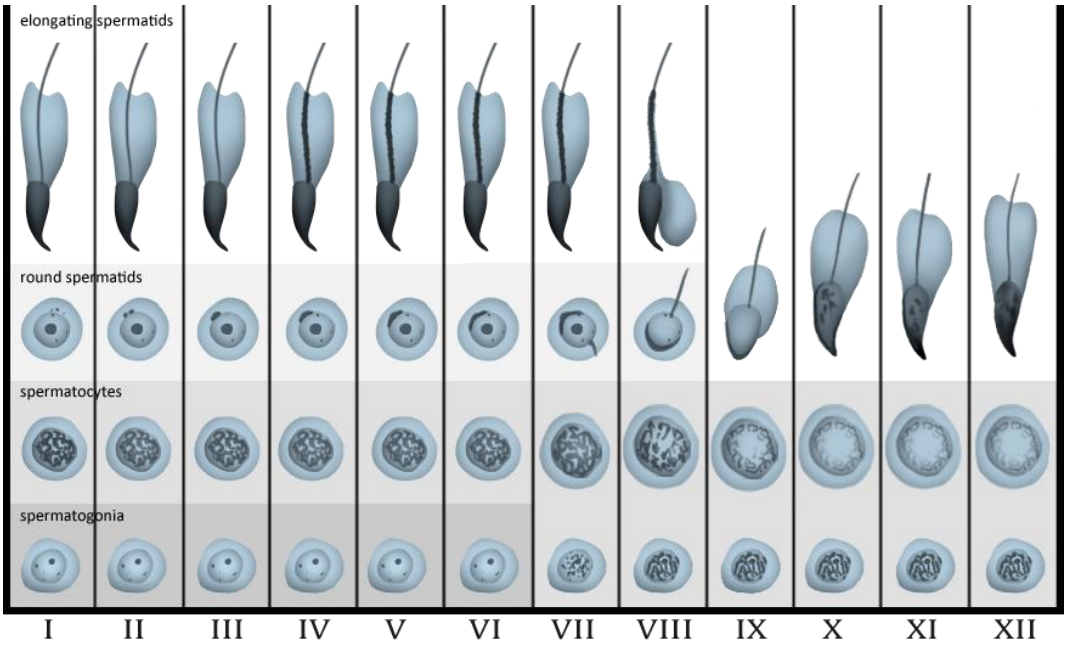

Figure 2. A diagram of the twelve stages of spermatogenesis in mouse. Each column represents a seminiferous tubule cross section at a different stage of the seminiferous epithelial cycle, demonstrating the stage-specific cell associations. The bottom layer of the diagram represents the least differentiated germ cells that reside closer to the basal lamina and in the top layer are the most differentiated germ cells nearing the tubule lumen. Earlier populations of spermatogonia are not shown in the diagram.

In the developing mouse testis, the first wave of spermatogenesis is initiated a few days after birth and is completed in postnatal week 6. Until postnatal day (PND) 7, only spermatogonia and Sertoli cells are present in the seminiferous tubules. At PND 9, the first early spermatocytes appear. At PND 20, as a result of spermatocytes undergoing meiosis, the first round spermatids appear. At PND 30, spermatid elongation begins and around PND 35, first mature spermatozoa are present in the testis. From hereafter, mature spermatozoa are continuously released from the seminiferous epithelium as the

spermatogenic wave proceeds and different segments of the tubule reach spermiation point. (Russell et al., 1987; Bellve et al., 1977; Laiho et al., 2013)

1.1 Spermiogenesis

The haploid germ cell differentiation programme, known as spermiogenesis, consists of 12 steps in human and 16 steps in mouse. In mouse, steps 1-8 comprise of round spermatid differentiation and steps 9-16 of spermatid elongation (Figure 3). During spermiogenesis, haploid germ cells undergo drastic cellular changes to transform into mature spermatozoa. This process is best characterized by the changing shape of spermatids from round to elongated, by compaction of the sperm head and formation of the sperm tail, but it involves many changes in cell organelles and molecular composition as well. (Russell et al., 1993)

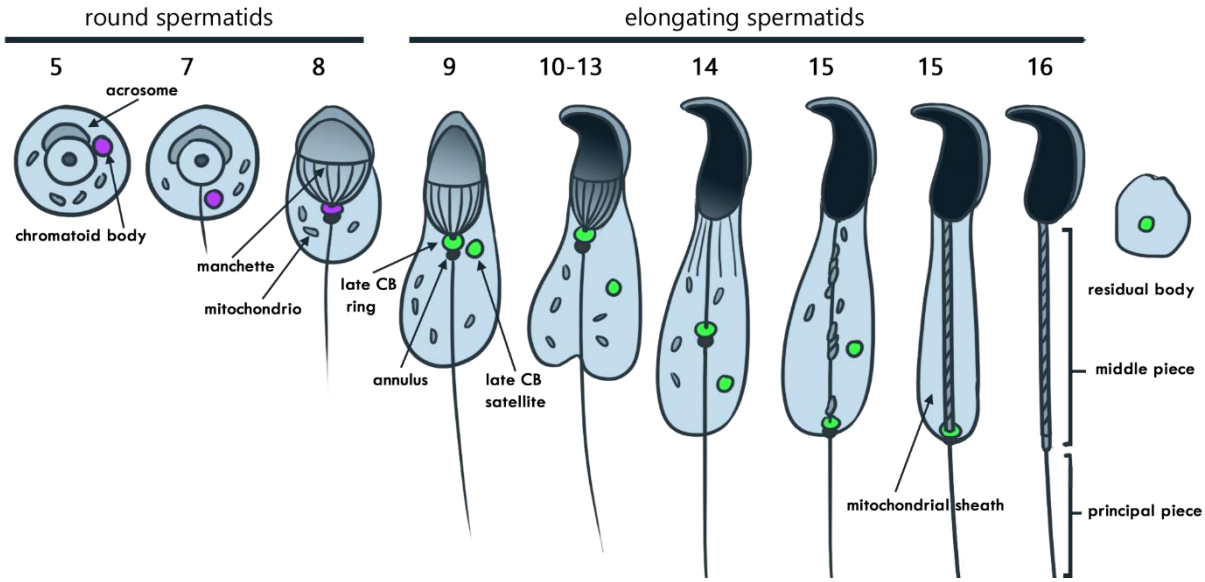

Figure 3. Overview of some central events of spermiogenesis. The acrosomal cap flattens in during round spermatid differentiation and obtains its final shape during spermatid elongation. In round spermatids, sperm tail accessory structures already start to arrange for the tail formation, after the core structure of the tail, the axoneme, is formed. The manchette is assembled at step 8 and disassembled at step 13-14. The CB (purple) is seen in round spermatids, and at step 8 it has migrated to the base of the flagellum. There it splits in two at step 9 spermatids, forming the late CB ring and satellite (green). The late CB ring migrates with the annulus to the end of the middle piece and the satellite stays cytoplasmic until step 16, when it is discarded with the residual body. Mitochondria assemble around the middle piece to form the mitochondrial sheath after the late CB ring and annulus have migrated to the end of the middle piece.

1.1.1 Acrosome formation and head shaping

Acrosome is a cap-like structure residing on the top of the sperm head that contains enzymes necessary for the fertilization, allowing spermatozoa to penetrate the oocyte. The acrosome is first present in step 1-2 spermatids as acrosomal vesicles formed by the Golgi complex (stage I-II) (Clermont and Leblond, 1955). At steps 3-5, the acrosome appears as a round shape in the cranial side of the nucleus, and in the following steps until step 8, it flattens and spreads along the nucleus. It is bound to the nucleus by a structure called acroplaxosome, and in the middle of the flattening acrosome, the acrosomal granule appears as a particularly dense spot. During spermatid elongation, from step 9 forward, the acrosome migrates to ventral position according to the nuclear shaping. The maturation phase of the acrosome, where it obtains its final form, corresponds to the maturation of elongating spermatids during steps 15 and 16. The Golgi complex, after first giving rise to the acrosome in the cranial side of the nucleus, then migrates to the caudal side of the nucleus in the beginning of spermatid elongation, at step 8. (Hermo et al., 2010c; Clermont and Leblond, 1955)

In step 1-8 round spermatids the nucleus has a round appearance but in steps 8-9 the nucleus starts to elongate (Hermo et al., 2010d). Inside the nucleus, chromatin is remodeled by removing histones and replacing them with protamines (Gatewood et al., 1987). Protamines pack the chromatin more tightly than histones, which results in nuclear condensation. Parallel to the nuclear condensation, a collection of microtubules starts to assemble around the nucleus. This microtubular structure is known as the manchette (Russell et al., 1991), and it spans from the basal body area in the caudal end of the nucleus to a perinuclear ring, opposing the acrosome. The manchette then migrates towards the tail, shaping the head as it progresses, until it is disassembled at steps 13-14. In addition to the shaping of the head, the manchette microtubules serve as a transport platform to deliver some sperm tail proteins to the caudally located basal body area, which is where the tail originates from (Lehti and Sironen, 2016).

1.1.2 Tail formation

The basal body is a pair of centrioles that form the first segment of the tail, the connecting piece (Chemes and Sedo, 2012). As the name suggests, the connecting piece is the structure that attaches the tail to the sperm head. This is achieved by the proximal centriole, that first migrates and attaches to the nucleus early in the spermiogenesis, in round spermatids. The distal centriole of the connecting piece polymerizes microtubules for the sperm tail core structure, the axoneme. The axoneme consists of nine microtubule

doublets that surround a central pair of single microtubules in a cylindrical form (Chemes and Sedo, 2012). The axoneme spans from the connecting piece to the following sperm tail segments: the middle piece, the principal piece, and the end piece. In the middle and principal pieces, the axoneme is surrounded by outer dense fibers that further support the tail. In the middle piece, there are 9 of these fibers, but in the principal piece, two of them are replaced by longitudinal columns of a fibrous sheath. The outer dense fibers and the fibrous sheath aid in supporting the tail structure and motility, but they have potentially many other roles in spermiogenesis as well (Lehti and Sironen, 2016).

The annulus is a ring-like structure encircling the axoneme, that is first seen in the beginning of spermatid elongation at the neck of the spermatid. It is attached to the inner side of the cell membrane and it draws the cell membrane to the sperm tail. As spermatid elongation proceeds to steps 14-15, the annulus migrates towards the principal piece, finally forming a junction and a diffuse barrier between the middle piece and the principal piece of the tail (Figure 3). Parallel to the migration of the annulus, begins the mitochondrial sheath formation. During steps 14-15, the mitochondria condense and migrate around the middle piece of the tail to form the helically structured mitochondrial sheath. (Kwitny et al., 2010; Ho and Wey, 2007)

As the spermatid elongation reaches its final steps and all the necessary tail and head structures are constructed and assembled correctly, residual cytoplasm gets discarded in step 16 spermatids. This residual body will be phagocytosed by Sertoli cells, and the spermiation can finally occur, releasing the mature spermatozoa to the lumen. (Hermo et al., 2010b)

Haploid male germ cells are also characterized by certain types of *nuage,* a cloud-like accumulations of electron dense material (Voronina et al., 2011). These cell organelles that are specific to germ cells are also known as germ granules. Next, one of the most distinguished of these germ granules, the chromatoid body (CB), will be discussed further.

1.2 The chromatoid body

The complexity of the spermatogenesis requires very specific and precise gene expression in each developmental phase. On top of this, the nuclear chromatin compaction and remodeling causes gene transcription to dramatically decrease and eventually cease during spermiogenesis (Gatewood et al., 1987). To ensure that a sufficient level of protein synthesis is maintained after this, haploid male germ cells need to store and process a

large number of gene transcripts (Soumillon et al., 2013). This poses a great challenge for efficient post-transcriptional and translational RNA control to regulate gene expression.

The germ granules that were mentioned before, are in fact male germ cell specific ribonucleoprotein (RNP) granules that serve to answer this challenge of RNA regulation (Voronina et al., 2011). RNP granules contain mRNA, noncoding RNA (ncRNA) and RNA-binding regulatory proteins, compartmentalizing and controlling many RNA regulatory pathways. Germ granules share many similarities with the RNP granules that are involved in the metabolism and degradation of RNA material in somatic cells, known as processing bodies or P-bodies, and stress granules. For example, all these RNP granules have been shown to store untranslated mRNA, RNA binding proteins and RNA helicases (Aizer et al., 2014; Jain et al., 2016). However, male germ cells have their own unique germ granules with unique functions.

The CB is a filamentous, granular structure that is most prominent during spermiogenesis in round spermatids (Fawcett et al., 1970). It is one of the first discovered germ granules, found and reported in the late 19th century in several different mammals including rat and mouse. Due to its relatively big size (⌀1-2 um) and electron density, the CB can be easily detected in electron microscopy (Figure 4A). The origin of the CB is thought to be in the intermitochondrial cement (IMC), which is also a type of nuage located within the mitochondrial clusters of primary spermatocytes (Lehtiniemi and Kotaja, 2018). As spermatocytes progress to the late pachytene, the CB condenses into a visible cytoplasmic bodies that fuse to a single granule right after meiosis. It is typically localized next to the nucleus, but there it can move along the nuclear envelope (Söderström and Parvinen, 1976). In later step round spermatids the CB usually moves away from the nucleus to the cytoplasm, and eventually it migrates to the caudal pole of the nucleus reducing in size, associating with the sperm tail in step 8 spermatids (Fawcett et al., 1970). Here the CB is finally divided into two succeeding structures, termed the late CB (Figure 4B).

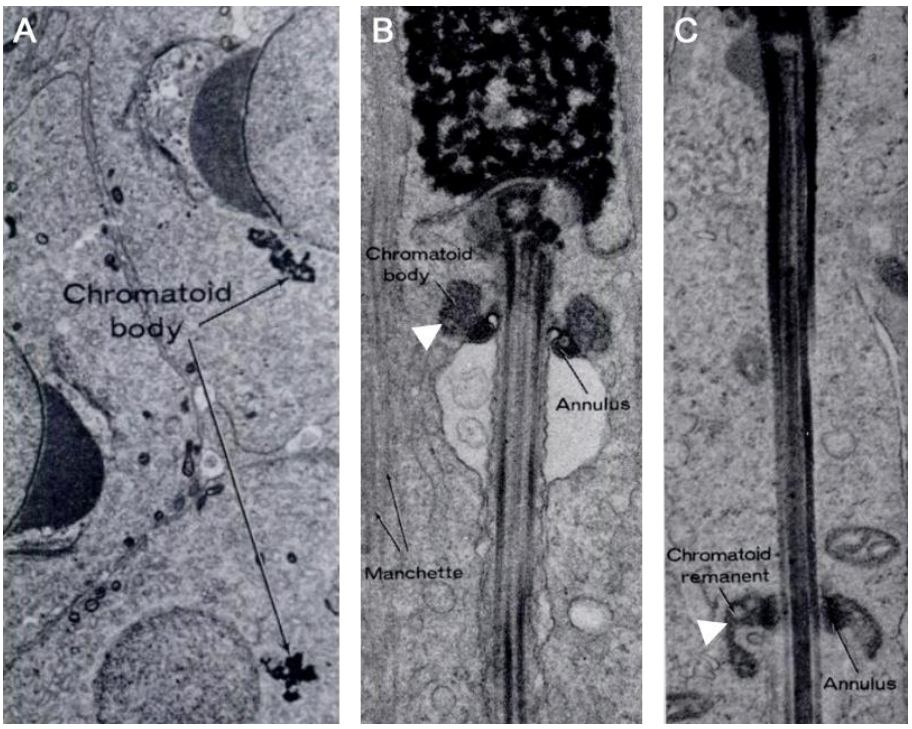

Figure 4. The CB and the late CB in electron microscopy. A) The CB is seen as a nuage of electron dense material near the nucleus. B) The late CB (white arrowhead) can be seen at the base of the flagellum adjacent to the annulus. C) As spermatid elongation proceeds, the late CB ring starts to migrate with the annulus to the caudal end of the middle piece. Image modified from Fawcett et al., 1970, with permission from the Oxford University Press.

Since the discovery of its components related to different ncRNA pathways, the CB has been recognized as a RNP granule that functions as an RNA processing center of the haploid male germ cells (Kotaja et al., 2006). The CB contains for example microRNAs (miRNAs), the RNA helicase VASA (or MVH for mouse VASA homologue) and Dicer, which is an endonuclease that processes miRNA precursors to mature miRNAs (Meikar et al., 2014). All of these are related to the miRNA and RNA interference (RNAi) pathways that control gene expression. Furthermore, the PIWI-interacting RNA (piRNA) pathway components, including the PIWI proteins MIWI (mouse PIWIL1) and MILI (mouse PIWIL2), and piRNAs (PIWI-interacting RNAs), are highly enriched in the CB (Meikar et al., 2014). The RNAi pathways mediated by miRNAs and Dicer are a means of posttranscriptional gene silencing, that results in cleavage of targeted mRNAs (Hannon, 2002). piRNA pathways, on the other hand, seem to have an independent function from the miRNA pathway, and are instead involved in silencing mobile genetic elements, such as transposons, as well as regulation of both protein coding and ncRNA expression (Aravin et al.). In terms of abundance, the main components of the CB are reportedly MVH, MIWI, TDRD6 (tudor domain-containing protein 6), TDRD7 and GRTH/DDX25 (gonadotropin

regulated testicular RNA helicase/DEAD-box helicase 25)(Meikar et al., 2014). TDRD6 has been associated with a nonsense-mediated RNA decay (NMD), suggesting that the CB also engages in NMD pathways (Fanourgakis et al., 2016). Other functions proposed for the CB include autophagy and protein degradation. The autophagy associated functions are mediated by FYCO1 (FYVE and coiled-coil domain containing 1) (Da Ros et al., 2017), whereas the presence and concentration of aggresome and ubiquitin pathway proteins in the CB suggests that it may act as a degradation site for proteins and RNA (Haraguchi et al., 2005).

The significance of the CB to spermatogenesis has been indicated with various genetically modified mouse models. For example, a mutation in MVH ATPase domain was reported to result in arrestment of spermatogenesis in the meiotic phase, before the CB is formed (Tanaka et al., 2000). In TDRD5, TDRD6 and TDRD7 knock-out (KO) mouse models, the CB is fragmented, and the mice are sterile (Yabuta et al., 2011; Vasileva et al., 2009; Tanaka et al., 2011). MIWI and MILI KO male mice have also been reported with sterile phenotypes, with the MIWI KO mouse displaying a disrupted CB architecture (Reuter et al., 2011; Unhavaithaya et al., 2009). These studies, among others, underline the importance of RNA regulatory pathways during spermatogenesis. However, the role of the CB itself in mediating these pathways is not fully elucidated yet. On top of this, in the middle of spermiogenesis, in step 8 spermatids, the CB transforms both structurally and functionally, and the main CB components disappear from the CB structure (Lehtiniemi and Kotaja, 2018). The structure that originates from the CB remnants is the much more elusive late CB.

1.3 The late chromatoid body

In step 8-9 spermatids the CB, that has now migrated to the connecting piece, splits in two (Figure 3) (Fawcett et al., 1970). One part of the CB remnants becomes a dense, cytoplasmic sphere from hereafter referred as the late CB satellite body. The other part stays in the connecting piece, where it forms a ring encircling the axoneme, localizing proximally next to the basal body and distally next to the annulus. This is the late CB ring. The satellite body remains in the cytoplasm where it appears to be able to move freely until the elongating spermatid maturation in step 16, when it gets discarded with the residual cytoplasm. The ring structure however closely associates with the annulus throughout spermatid elongation: in step 14-15 spermatids it starts to migrate with the annulus along the axoneme, parallel to the mitochondrial sheath formation. In step 15

spermatids the ring can be eventually seen in the middle-principal piece junction of the tail, next to the annulus, until it disappears from step 16 elongating spermatids. (Fawcett et al., 1970; Lehtiniemi and Kotaja, 2018)

Parallel to the structural changes that take place during the transformation of the CB into the late CB, compositional changes take place as well. The piRNA pathway related proteins and other main CB components, including DDX4, DDX25 and TDRD6, disappear from both late CB structures, the ring and the satellite body (Shang, 2014). In addition, some proteins that are not detected in the CB of round spermatids, start to accumulate in the late CB structures. These are two members of the testis-specific serine/threonine kinase (TSSK) family, TSSK1 and TSSK2, and their substrate testis-specific kinase substrate (TSKS) (Shang et al., 2010). TSSK1, TSSK2 and TSKS can all be detected from the cytoplasm of elongating spermatids, but their expression is most concentrated and prominent in both the late CB ring and the satellite body. This accumulation of these three proteins in the late CB ring and satellite can first be seen in step 8-9 spermatids and they remain in the late CB structures until elongating spermatid maturation.

The role of the late CB in spermatid elongation has long remained unexplored and elusive. However, the specificity of TSSK1 and TSSK2 to the late CB has enabled some recent discoveries that in part elucidate its function during spermiogenesis. A double KO mouse model with *Tssk1* and *Tssk2* genes tandemly silenced was developed by Shang et al., 2010. This study demonstrated that the TSSK1/2 KO male mice were infertile and has notable morphological abnormalities in the epididymal spermatozoa. Early spermiogenesis was unaffected, but some disorganization and excess cytoplasm was seen in later step elongating spermatids. The most remarkable defect was found to be in the mitochondrial sheath formation, as the mitochondria were mostly staggered in clusters near the connecting piece of tail, instead of organizing around the outer dense fibers of the middle piece to form the mitochondrial layer. In step 15 spermatids of the TSSK1/2 KO mice, the electron dense material that resembles the late CB was not observed next to the annulus, as compared to the wild type (WT) mouse spermatids. In earlier step spermatids, some accumulation of TSKS was found in structures resembling the late CB ring and satellite, but this accumulation disappeared in step 13 and TSKS was dispersed throughout cytoplasm. These findings suggest that TSSK1 and TSSK2 and are essential for the late CB as it starts to migrate towards the caudal end of the middle piece, and this phenomenon, or the related activity of TSSK1 and TSSK2, appears to be essential for the mitochondrial sheath formation. (Shang et al., 2010)

1.4 Testis-specific serine/threonine kinases

TSSK1 and TSSK2 belong in a family of six testis-specific serine/threonine kinases (TSSKs), TSSK1-6, that in turn belong into a superfamily of calcium/calmodulin-dependent protein kinases (CaMKs). The expression of TSSKs is specific to the testis and spermatogenesis, indicating their importance to male reproductive health. The firstly discovered members of the TSSK family were TSSK1 and TSSK2, as the genes *Tssk1* and *Tssk2* encoding these proteins were cloned in 1990s. The mouse genes *Tssk1* and *Tssk2* are syntenic, residing in very close proximity to each other in chromosome 16. In human, however, *Tssk1* is replaced by a pseudogene *TSSK1A* that does not encode an active protein, and instead humans have an active TSSK1B protein encoded by *TSSK1B* that resides in a different genomic region to *Tssk2*. Other than this exception in human and some other primates, *Tssk1* and *Tssk2* are conserved genes expressed in all mammalian species. (Salicioni et al., 2020)

As kinases, TSSK1 and TSSK2 among other TSSKs act mainly as phosphorylating enzymes, sharing the same conserved catalytic domain (Li et al., 2011). In addition to synteny of the genes, TSSK1 and TSSK2 are highly homologous structurally and functionally. They are shown to interact with each other, in addition to their shared substrate, TSKS (Kueng et al., 1997; Xu et al., 2007). They phosphorylate TSKS at Ser-285, and in order to be active, they can autophosphorylate themselves (Xu et al., 2008a; Li et al., 2011). Phosphorylation is a fundamental mechanism of signal transduction in many molecular pathways of the cell, and most typically it is done as a post-translational modification that alters the activity of newly translated proteins. Altogether, kinases are one of the largest gene families in eukaryotes, highlighting their role in cellular processes such as metabolism, differentiation, molecular transport and motility (Ubersax and Ferrell, 2007). This further implicates the importance of TSSKs for spermatogenic processes. However, much of the functions of these proteins during spermatogenesis still remains unknown.

As discussed earlier, the TSSK1/2 KO model demonstrated that TSSK1 and TSSK2 are associated with the late CB and mitochondrial sheath formation (Shang et al., 2010). Another study found a similar linkage to mitochondrial sheath formation between TSSK1, TSKS and testis-specific phosphatase PPP1CC2 (MacLeod et al., 2014). PPP1CC2 is testis-specific protein phosphatase that is expressed only in male germ cells and in cytoplasmic regions (Sinha et al., 2012). However, TSSK1 and TSKS appear to be upstream regulated by PPP1CC2, as their localization to the late CB was decreased in

PPP1CC2 null mice (MacLeod et al., 2014). In the same KO mouse model, the interplay of these three proteins as a kinase/phosphatase complex was demonstrated to be crucial for the organization of the mitochondrial layer. Other functions of TSSK2 may relate to the flagellar motility, as it has been reported to phosphorylate SPAG16L, an axonemal protein that is involved in sperm motility (Zhang et al., 2008). In line with this finding, SPAG16L KO mice have significantly decreased levels of testicular TSSK2 expression. A mouse model with targeted mutation in SPAG16L demonstrated, that mice with deficient SPAG16L are infertile due to defects in sperm motility and reduced sperm count (Zhang et al., 2008). Intriguingly, sperm tail morphology and spermatogenesis were nevertheless mostly undisturbed in the SPAG16L deficient mice.

A Gene Ontology (GO) analysis has been performed to interaction candidates of TSSK1/2 and TSKS, discovered by mass spectrometry of co-immunoprecipitated protein complexes (Shang, 2014). The GO analysis provided evidence that TSSK1, TSSK2 and TSKS are all involved in RNA related processes, but they also have differential roles for example in protein transport (TSSK1 and TSSK2), mitochondria (TSSK1 and TSSK2) and cytoskeletal processes (TSSK1 and TSKS). Furthermore, TSSK2 was found to have GO analysis supported activity in protein phosphorylation and kinase function, whereas this linkage was not found with TSSK1. Finally, as TSKS has been shown to localize in the centrioles during spermiogenesis, it is possible to speculate that TSSK1 and TSSK2 have also an association to centriole function via TSKS (Xu et al., 2008b). As centrioles are involved in the intramanchette and intraflagellar transport, it could be speculated that protein phosphorylation takes place in the centriole to post-translationally modify the proteins that are transported from the head to the tail (Deane et al., 2001; Xu et al., 2008b).

Other TSSKs appear to have distinct, specialized roles in spermatogenesis as well. This is supported by the varying expression patterns of TSSKs during spermatogenesis and in mature spermatozoa (Li et al., 2011; Salicioni et al., 2020). In the seminiferous epithelium of the testis, TSSK1 and TSSK4 have been reported to be expressed in spermatogonia and elongating spermatids, but not in round spermatids. Although one study found TSSK4 to be expressed in round spermatids as well, and in elongating spermatids TSSK4 was shown to be expressed in more concentrated foci (Wei et al., 2013). This localization, however, was not reported to reside in the late CB. TSSK2 and TSSK6 on the other hand have been reported to be expressed only in elongating spermatids. TSSK3 protein expression in the testis has not been demonstrated, but the gene *Tssk3* is transcribed in postmeiotic germ cells. In mature mouse spermatozoa, TSSK1 and TSSK4 again share a

similar expression patterns, localizing in the whole tail region and the acrosome. TSSK2 and TSSK6 are reportedly expressed in postacrosomal/caudal region of the sperm head. (Li et al., 2011; Salicioni et al., 2020)

In addition to the TSSK1/2 KO, TSSK4 KO and TSSK6 KO have been described in literature as well (Wang et al., 2014; Sosnik et al., 2009). TSSK4 null mice were subfertile, with lacking microtubule(s) in the central axonemal pair, and abnormalities in the junction between the middle piece and the principal piece (Wang et al., 2014). These abnormalities resulted in motility defects of the spermatozoa (Wang et al., 2014). TSSK6 null male mice were infertile, and the spermatozoa had notable morphological abnormalities (Sosnik et al., 2009). The acrosome reaction of the spermatozoa was also defected, preventing the fertilization to occur. Altogether, the infertile phenotypes of TSSK1/2 KO and TSSK6 KO mice and the subfertile phenotype of TSSK4 KO mice highlight the significance of TSSK proteins to spermatogenesis.

Due to its close association with the late CB and male reproductive health, TSSK2 was chosen as the focus of this study. A novel interaction candidate for TSSK2 was discovered: eIF3 complex, which is a key factor in translation initiation (Hinnebusch, 2006). We investigated the interplay between TSSK2 and eIF3 during spermatid elongation, and the potential connection between the late CB and translation regulation. Hereby, we propose that TSSK2 interacts with eIF3, and the late CB function is connected to translation and RNA regulation of male germ cells.

2. Results

2.1 TSSK2 localizes to the late CB in elongating spermatids

First, to examine the cellular expression of TSSK2 in testis during different stages of spermatogenesis, immunofluorescence staining was performed on WT mouse testis cross-sections (Figure 5). All specific TSSK2 signal was localized proximal to the seminiferous tubule lumen, expressed only in elongating spermatids, as described in the literature(Salicioni et al., 2020). However, the expression pattern changes markedly as spermatid elongation proceeds. The transformation of the CB into the late CB takes place around stage IX in step 9 spermatids, and this is where concentrated TSSK2 staining can be first seen in the ring and the satellite body structures, that are located near each other in the neck of the spermatids (Figure 5A). During the following steps of spermatid elongation, in step 13-14 spermatids the satellite body migrates further in the cytoplasm,

but the ring structure remains in the neck (Figure 5B). In step 15 spermatids, the ring structure migrates along the middle piece to the caudal end of the middle piece where the principal piece begins (Figure 5C). Finally, both signals diffuse into a more homogenic, cytoplasmic TSSK2 staining in the remaining and residual cytoplasm of elongating spermatids until spermiation takes place (Figure 5D).

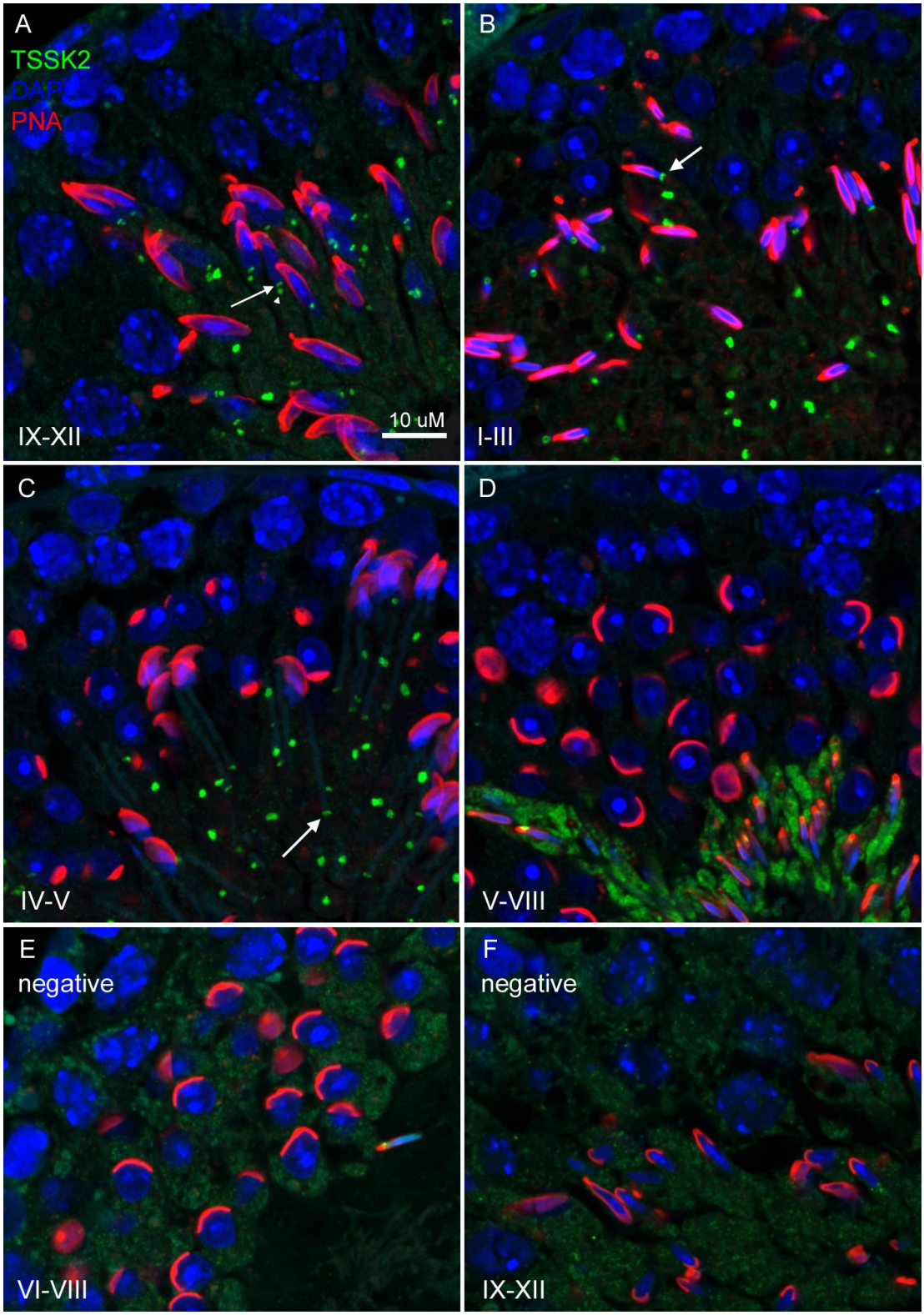

Figure 5. TSSK2 localization in WT testis sections at different stages of seminiferous epithelial cycle. In all stages, TSSK2 (green) is expressed specifically in elongating spermatids next to the seminiferous tubule lumen, but its expression pattern changes notably during spermatid elongation from the concentrated late CB structures (arrows) to more diffuse and cytoplasmic localization. A) The late CB can first be seen right in stages IX-XII, where the ring structure (arrow) is located in the neck of the spermatid and the satellite body (arrowhead) is in very close proximity to the ring structure. B) As spermatid elongation progresses, in stages I-II the ring structure remains in the neck (arrow) whereas the satellite body migrates further away in the cytoplasm. C) In stages III-V the ring structure migrates to the caudal end of the middle piece (arrow), where it can be seen until stages VI-VIII. D) In VI-VIII, TSSK2 is still present in elongating spermatid cytoplasm but is no longer concentrated to the late CB. E) and F) show negative controls of stages VI-VIII and IX-XII, respectively, with only faint background autofluorescence present. Nuclei are stained with DAPI (blue) and acrosome with PNA (red).

To further examine the intracellular localization of TSSK2, immunofluorescence was performed on isolated germ cells of drying down preparations (Figure 6). TSSK2 signal was detected in the late CB ring, first in the neck of the spermatid in step 12-13 elongating spermatids of stage XII-I, and later in the caudal end of the middle piece in step 15 spermatids of stage V-VI. TSSK2 was also seen as dispersed, cytoplasmic staining especially in the middle piece and head of step 15 spermatids. This is in line with what was seen in the testis cross-sections. Additionally, in step 16 spermatids an accumulation of TSSK2 was seen in caudal region of the sperm head and under the acrosome, where TSSK2 staining followed the shape of the acrosome. In step 16 spermatids, corresponding to stages VII-VIII, the late CB ring has already disappeared.

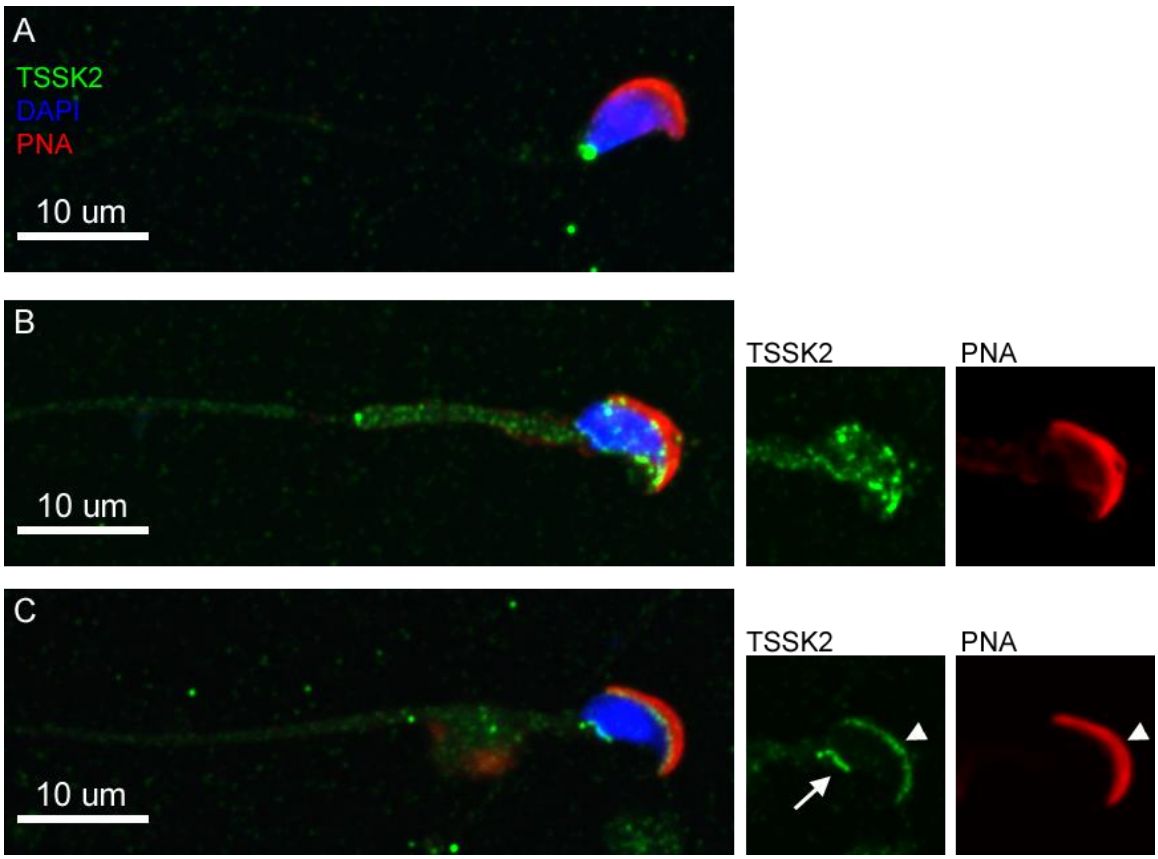

Figure 6. TSSK2 immunofluorescence on isolated spermatids. TSSK2 (green), DAPI stained nuclei (blue) and PNA stained acrosome (red) in drying down preparations of isolated elongating spermatids. A) In step 12-13 elongating spermatids, TSSK2 stains the late CB ring (arrowhead) in the neck of the spermatids. B) As elongation proceeds to step 15 spermatids, the late CB ring is seen in the caudal end of the middle piece. A more dispersed TSSK2 signal is also detected in the middle piece and the head of the spermatid, where it appears to partly overlap with the acrosomal staining (insert). C) In step 16 spermatids the late CB ring has disappeared from the tail. In the sperm head, TSSK2 signal can be detected right under the acrosome (insert, arrowhead), following the curved shape. TSSK2 is also present in the caudal region of the sperm head (insert, arrow).

2.2 Preparation of TSSK2 complexes for mass spectrometry

After the TSSK2 antibody was validated to work in immunofluorescence and to detect the late chromatid body ring and satellite structures with good accuracy, it was used to co-immunoprecipitate TSSK2 interacting proteins (Figure 7). The aim was to pull down TSSK2 interaction candidate proteins and to analyze the precipitated protein complexes with mass spectrometry for novel information on the late CB protein composition and thereby its function in spermatogenesis. Two biological replicates were prepared using two independent mice. Mouse IgG IP was used as a negative control. After co-IP had been performed, the outcome of the experiment was examined by western blotting with TSSK2

antibody. A signal was detected at 37 kD, which corresponds to the expected size of TSSK2 (39 kD), in both lysate and TSSK2 IP samples, with the IP bands being much stronger. Mouse IgG IP samples gave no signal at the size of 37 kD, confirming that the TSSK2 IP had been successful.

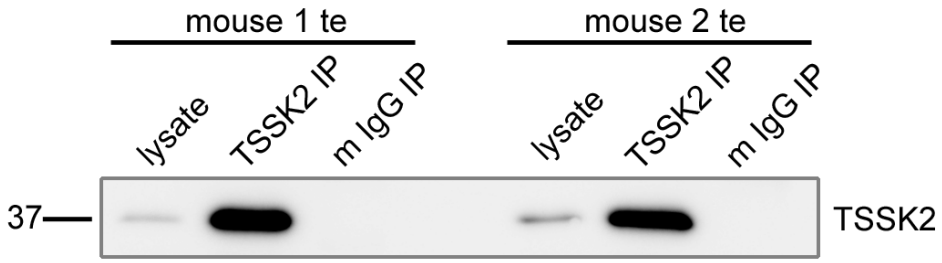

Figure 7. Western blot of the TSSK2-coIP samples that were used for mass spectrometry analysis. Samples from two different mice were used. Lysates and TSSK2 IP samples gave defined, specific bands corresponding to the expected size of TSSK2 (39 kD), although the TSSK2 IP bands were considerably stronger. Negative control mouse IgG IP samples were empty at 37 kD.

A silver staining of SDS-PAGE gel was also performed to examine the protein content in the IP samples before the western blot (Figure 8). The results of the silver staining showed that an abundance of proteins was present in the lysate and the IP sample. Strong bands corresponding to the heavy and light Ig chains were detected from the TSSK2 IP and mouse IgG IP both, but the overall amount of protein in the samples was higher in the TSSK2 IP sample and it showed more specific staining compared to mouse IgG IP.

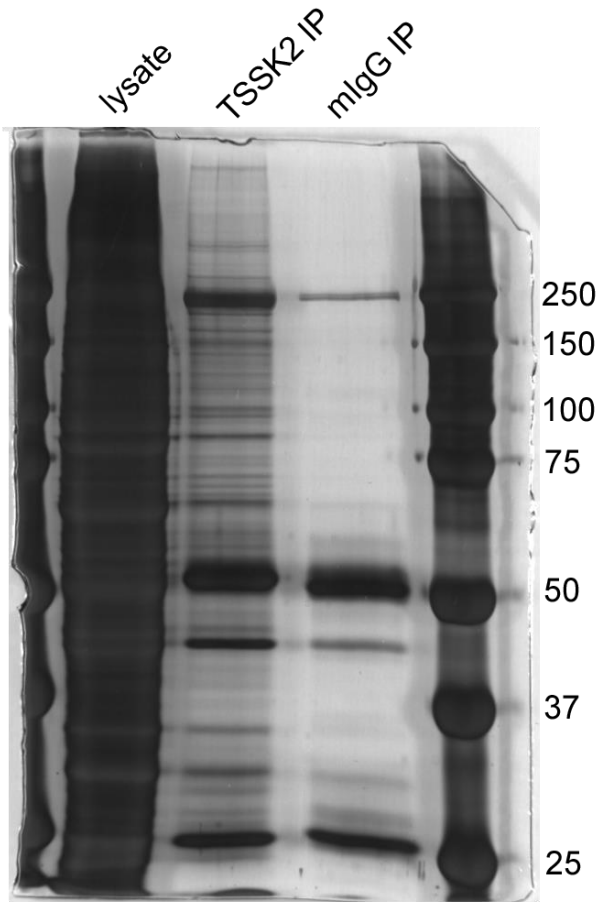

Figure 8. Silver staining of the SDS-PAGE gel with resolved lysate and IP samples. Protein contents of the gel are stained with dark grey. The lysate contains a large amount of all kinds of testicular proteins, resulting in a rather uniform, dark and saturated coloring of the whole sample. In both the TSSK2 IP and mouse IgG IP samples, dark bands of 50 kD correspond to the Ig heavy chains and bands of 25 kD to the Ig light chains. Other distinguishable bands are more or less specific to TSSK2 IP, with higher intensity in the TSSK2 IP sample compared to the mouse IgG IP.

2.3 TSSK2 interacts with eIF3 translation initiation complex

When the immunoprecipitation had successfully been performed, the IP-beads were analyzed with mass spectrometry. Protein hits that were found from only one of the two TSSK2 IP samples or mouse IgG IP sample were removed from further analyses, leaving 288 proteins as a result. TSSK2 and its known interaction candidates TSSK1 (Kueng et al., 1997) and TSKS (Xu et al., 2007) were all present in significant number of peptides with high coverage confirming the analysis true and successful (Table 1). One remarkable finding was that the mass spectrometry analysis detected a considerable number of translation-related proteins. Eukaryotic translation initiation factor 3 (eIF3) complex was among the most abundant proteins detected, with 11 out of 13 subunits present in the analysis. eIF3a was the most copious of these subunits, with 83 peptides in one sample

and 34 in the other one. Other translation related proteins detected in the analysis included multiple 40S and 60S ribosomal subunit proteins, elongation factor 1 subunits and two ATP-dependent RNA helicases that are all involved in translation. A selection of the relevant mass spectrometry findings is presented in the table below.

Table 1. Mass spectrometry results of TSSK2-coIP. Results of the mass spectrometry analysis are presented in the table below. The presence of TSSK1, TSSK2 and TSKS, that are known to interact with together, aided to validate the results of the IP and mass spectrometry. An intriguing prevalence of translation-associated proteins was discovered, including 11 out of 13 of the eukaryotic initiation factor 3 complex and an abundance of both 40S and 60S ribosomal subunit proteins. Gn = gene name, coverage = sequence coverage of the matched peptides of the total protein sequence in the database, peptides = the number of distinct peptide sequences in the protein group.

		mouse 1		mouse 2	
Gn		**coverage**	**peptides**	**coverage**	**peptides**
Tsks	Testis-specific serine kinase substrate	68	43	69	44
Tssk2	Testis-specific serine/threonine-protein kinase 2	49	25	63	26
Tssk1b	Testis-specific serine/threonine-protein kinase 1	51	16	51	15
Eif3a	Eukaryotic translation initiation factor 3 subunit A	52	84	26	34
Eif3b	Eukaryotic translation initiation factor 3 subunit B	52	37	24	13
Eif3c	Eukaryotic translation initiation factor 3 subunit C	48	43	15	11
Eif3d	Eukaryotic translation initiation factor 3 subunit D	56	26	28	11
Eif3e	Eukaryotic translation initiation factor 3 subunit E	36	20	10	4
Eif3f	Eukaryotic translation initiation factor 3 subunit F	28	9	7	2
Eif3g	Eukaryotic translation initiation factor 3 subunit G	55	16	28	4
Eif3h	Eukaryotic translation initiation factor 3 subunit H	32	14	20	6
Eif3i	Eukaryotic translation initiation factor 3 subunit I	60	18	34	9
Eif3k	Eukaryotic translation initiation factor 3 subunit K	28	6	10	2
Eif3l	Eukaryotic translation initiation factor 3 subunit L	46	24	14	6
Eif4a1	Eukaryotic initiation factor 4A-I	17	5	10	3
Eif4g1	Eukaryotic translation initiation factor 4 gamma 1	26	37	6	7
Eif4g3	Eukaryotic translation initiation factor 4 gamma 3	25	33	7	11
Eif4b	Eukaryotic translation initiation factor 4B	16	7	9	3
Eif5a	Eukaryotic translation initiation factor 5A-1	30	3	30	3
Rps11	40S ribosomal protein S11	63	12	58	11
Rps18	40S ribosomal protein S18	59	11	59	10
Rps19	40S ribosomal protein S19	59	10	56	10
Rps3a	40S ribosomal protein S3a	66	17	62	19
Rpl10	60S ribosomal protein L10	45	9	61	13
Rpl12	60S ribosomal protein L12	66	7	55	7
Rpl23	60S ribosomal protein L23	54	8	48	7
Rpl24	60S ribosomal protein L24	53	9	50	8
Rpl30	60S ribosomal protein L30	59	5	51	4
Rpl31	60S ribosomal protein L31	53	7	45	6
Rps27a	Ubiquitin-40S ribosomal protein S27a	49	7	51	8
Uba52	Ubiquitin-60S ribosomal protein L40	31	3	35	5

Eef1a1	Elongation factor 1-alpha 1	38	19	27	8
Eef1d	Elongation factor 1-delta	14	3	14	3
Eef1g	Elongation factor 1-gamma	30	11	6	2
Ddx1	ATP-dependent RNA helicase DDX1	16	9	9	6
Ddx3x	ATP-dependent RNA helicase DDX3X	23	13	24	14

Given the abundancy of eIF3 subunits in the mass spectrometry analysis, this protein complex was chosen as the lead candidate for further research on the late CB. As eIF3 is vital in the initiation of protein translation from RNA transcripts, a hypothesis was formed that the late CB is involved in RNA regulation during spermatid elongation.

2.4 Validation of the interaction between TSSK2 and eIF3a

To confirm and validate the results of the MS analysis, the protein-protein interaction of eIF3a and TSSK2 was studied with co-IP. Western blots of the immunoprecipitated protein complexes are shown in Figure 9. TSSK2 was successfully pulled down from TSSK2 IP and lysate, as demonstrated earlier in the mass spectrometry IPs. eIF3a IP was also confirmed to work with eIF3a probe, although eIF3a band from the lysate was faint. When TSSK2 IP was probed with eIF3a antibody, a faint but distinct, specific band was detected at 150 kD validating the hypothesis that the two proteins interact at least moderately. TSSK2 band was however not detected from eIF3a IP.

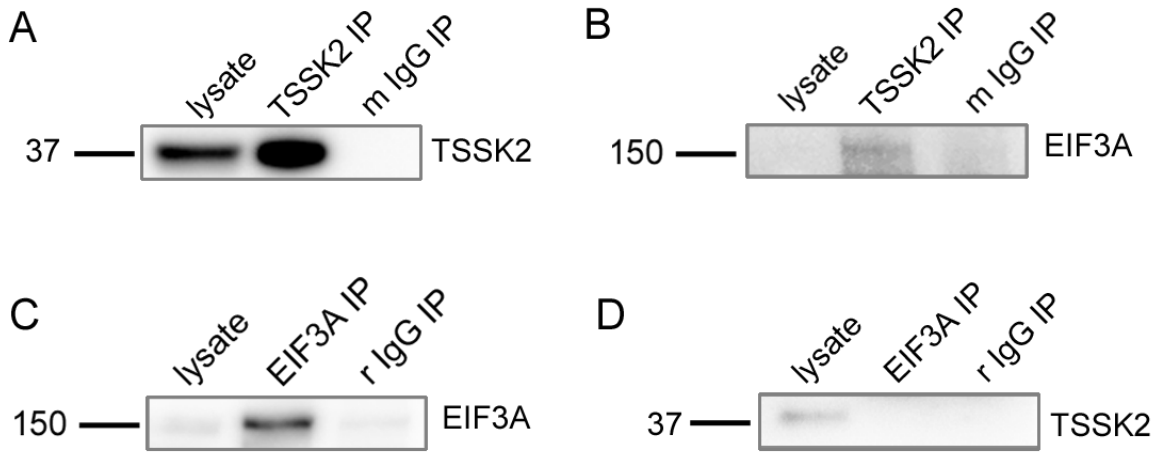

Figure 9. Western blot of co-immunoprecipitations with TSSK2 and eIF3a. A) TSSK2 is seen in the ~37 kD bands in the testis lysate and TSSK2 IP as excepted, whereas the negative control mouse IgG IP is empty. B) eIF3a (167 kD) is detected in a band around a 150 kD size mark from the TSSK2 IP, although lysate is clear. C) eIF3a is detected from eIF3a IP sample, but only faintly in the lysate. D) Lysate gives appropriate TSSK2 signal, but EIF3a IP is empty.

2.5 Expression of TSSK2 and eIF3a during the first wave of spermatogenesis

To investigate if the expressions of TSSK2 and eIF3a temporally overlap during the first wave of spermatogenesis, western blotting was performed on testis samples collected at different postnatal time points (1, 2, 3, 4, 5, 7 and 12 weeks) (Figure 10). TSSK2 specific 39 kD-sized band is first detected in 5-week old testis lysate, in line with spermatid elongation beginning around week 4 or 5 postpartum for the first time in developing testes (Bellve et al., 1977). The bigger bands around 150 and 250 kD are unknown and a few smaller unspecific bands are also seen in week 1 and week 2 testes. eIF3a, however, is detected consistently from the week 1 to week 12 postpartum at 150 kD. Several smaller bands appear with equal consistency under the eIF3a specific bands, but these are much weaker than eIF3a and presumably detect some eIF3a isoforms or partly degraded proteins. GAPDH (36 kD) was used as a loading control in both membranes after stripping the original antibody off. GAPDH staining reveals some minor variability between the protein amounts in the samples but it is mostly uniform and verifies the blotting successful.

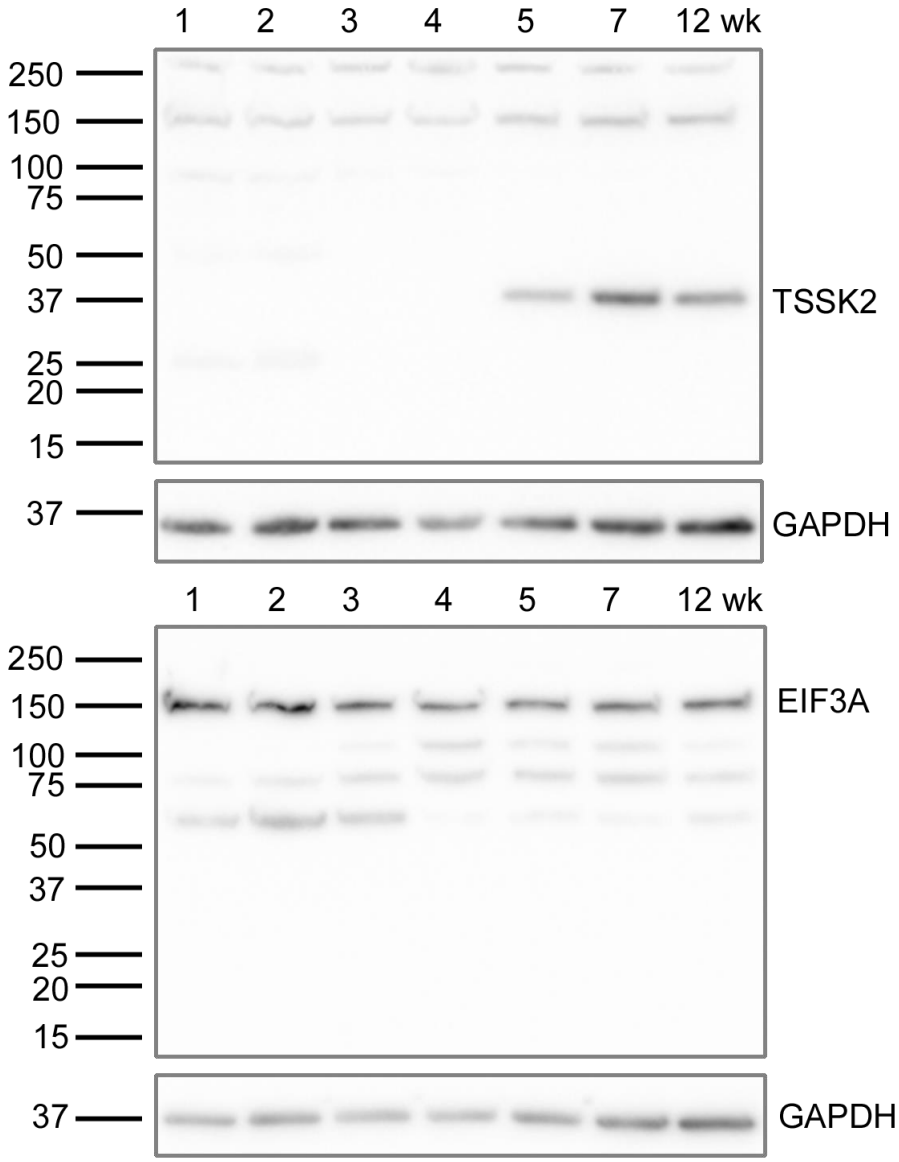

Figure 10. Western blots of TSSK2 and eIF3a in developing mouse testes from week 1 to week 12. TSSK2 is first expressed in week 5 in line with the start of spermatid elongation in the testes, whereas eIF3a is continuously expressed throughout the maturing of the testes. GAPDH below each membrane is used as a loading control after stripping the original membrane.

2.6 eIF3 localization transiently associates with TSSK2-positive late CB at specific steps of differentiation

Next, to characterize the cellular localization of the two proteins TSSK2 and eIF3a together, an immunofluorescence staining in WT mouse testis cross-section was performed (Figure 11). TSSK2 signal was identical to that observed in the previous immunofluorescence stainings, localizing in the elongating spermatids only. eIF3a staining, on the other hand, was visible and uniform in all cell types, giving mostly a diffuse, cytoplasmic signal throughout all stages of spermatogenesis. In stages I-II, however, the

signals of TSSK2 and eIF3a could often be seen in close proximity to each other and sometimes overlapping. Interestingly, this association with the late CB is transient and soon disappears when spermatogenesis proceeds to next stages. Furthermore, the eiF3a and TSSK2 signals do not completely overlap, but they are still next to each other and closely associated.

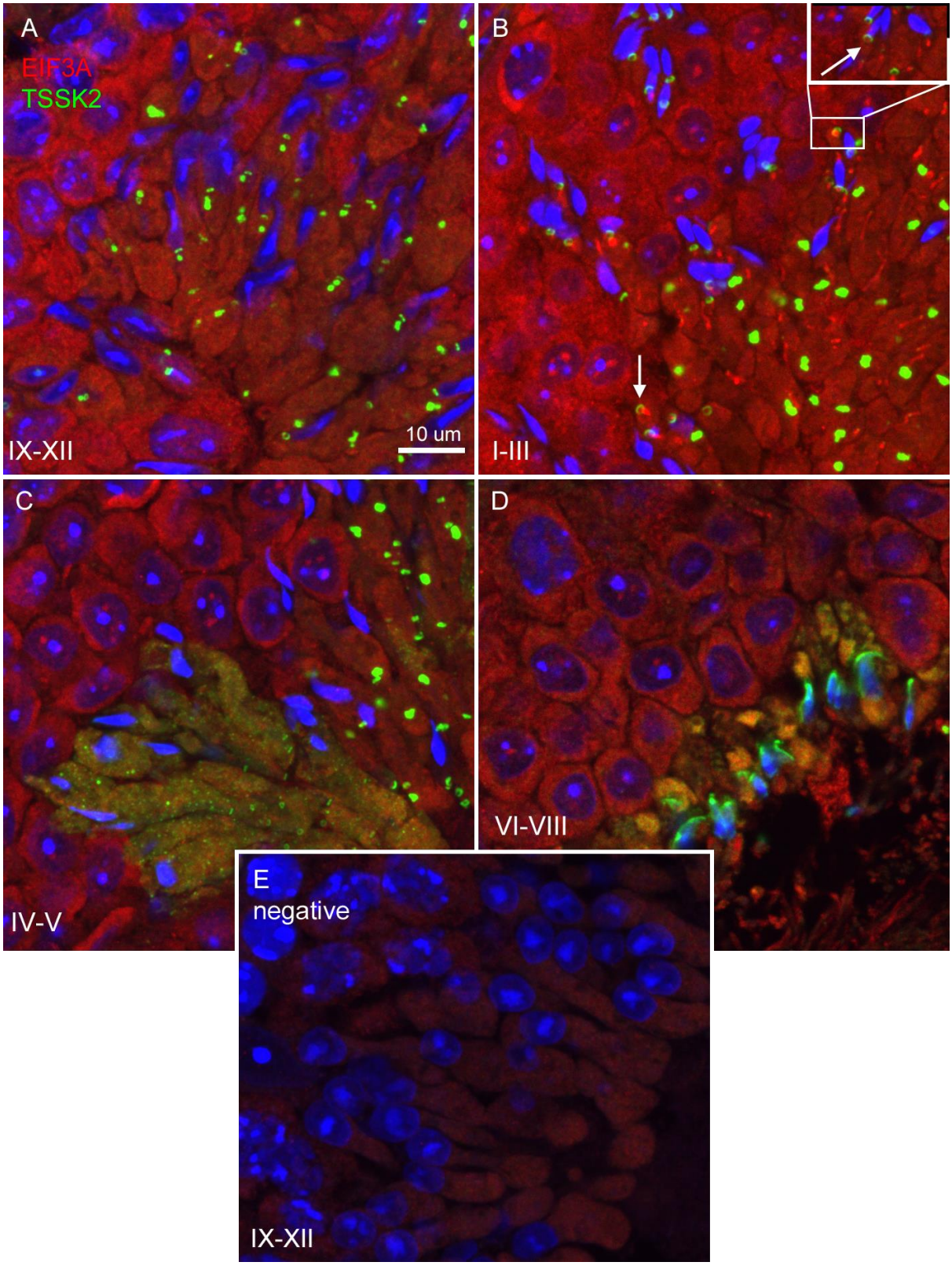

Figure 11. TSSK2 and eIF3a localization in WT mouse testis sections during different stages of spermatogenesis. A) TSSK2 (green) localizes to the transforming and migrating late CB structures, the ring and the satellite body, whereas eIF3a expression is more diffuse and cytoplasmic. B) In stages I-II in step 12-13 elongating spermatids eIF3a gives more specific signal near tubule lumen, as concentrated dots or lines. These concentrated sites can be often detected overlapping with TSSK2 signal, examples marked by the two white arrows. C) Stages IV-V show again more cytoplasmic and dispersed eIF3a expression while TSSK2 is also diffusing to the cytoplasm. D) TSSK2 is concentrating to acrosomal regions of step 16 elongating spermatids. Some TSSK2 signal remains in the residual cytoplasm, where eIF3a can also be seen, and the yellowish color suggests some overlapping of the signals in the cytoplasm. E) Negative control has no specific signal.

eIF3a antibody from another manufacturer (Sigma Aldrich) was needed for some following experiments and was therefore also tested on IF (Figure 12). The results of the new antibody in WT mouse testis cross-section IF were mostly uniform with the previous antibody, although the accumulations of eIF3a signal associated with the late CBs were smaller in size.

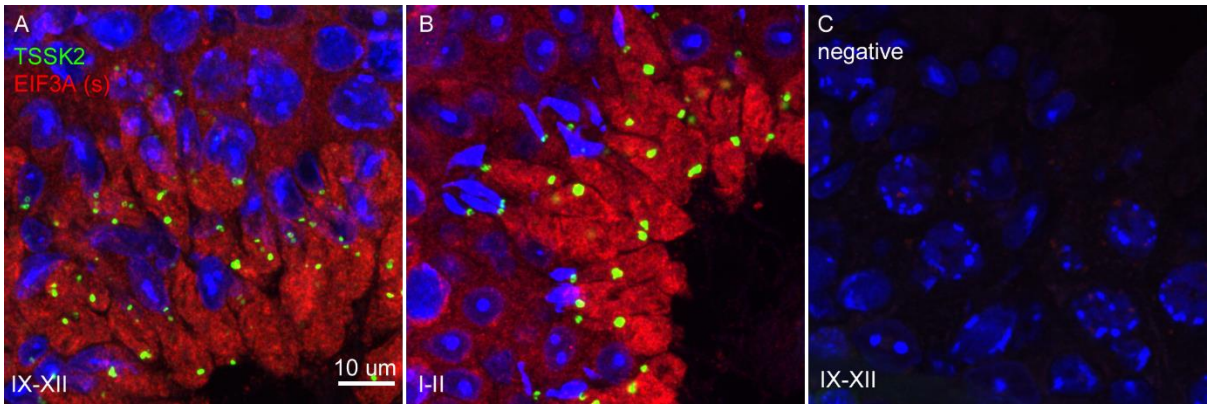

Figure 12. eIF3a (sigma) in testis. TSSK2 (green) staining is again comparable to previous results. eIF3a (sigma) is diffuse, cytoplasmic and covers all cell types of the testis with similar expression pattern throughout all stages of spermatogenesis. Stages IX-XII (A), I-II (B), and a negative control (C) are presented here for reference. No exact co-localization with TSSK2 was detected, but in stages I-II eIF3a (sigma) is appears to localize more intensively in elongating spermatids near the lumen.

Another eIF3 complex subunit eIF3f was investigated in immunofluorescence with TSSK2 to support the findings with eIF3a and further investigate the association between eIF3 complex and TSSK2. WT mouse testis cross-sections were stained with eIF3f and TSSK2 (Figure 13). Mostly cytoplasmic and diffuse eIF3f was detected in all cell types throughout spermatogenesis, but in stage IX-XII it formed more concentrated patterns overlapping

with TSSK2 staining. This co-localization takes place mostly in the satellite structure of the late CB, as can be seen in Figure 14. Some faint overlapping signal can be seen at the site of the late CB ring as well, but the intensity of the eIF3f is not as strong as in satellite body and is not easily distinguished from the diffuse cytoplasmic eIF3f signal. This pattern of co-localization could be seen only during stages IX-XII. Another novel finding from eIF3f IF, accompanied with acrosomal PNA staining, was that eIF3f formed concentrated dots overlapping with acrosomal granules (Figure 15). This was seen especially during stages II-VII, appearing when the acrosome is first formed, and disappearing parallel to the acrosomal granule. Overall, the results of eIF3f and TSSK2 IF were mostly comparable to eIF3a and TSSK2, but with some distinctive features such as the possible co-localization appearing earlier in spermatid elongation, and the acrosomal overlap.

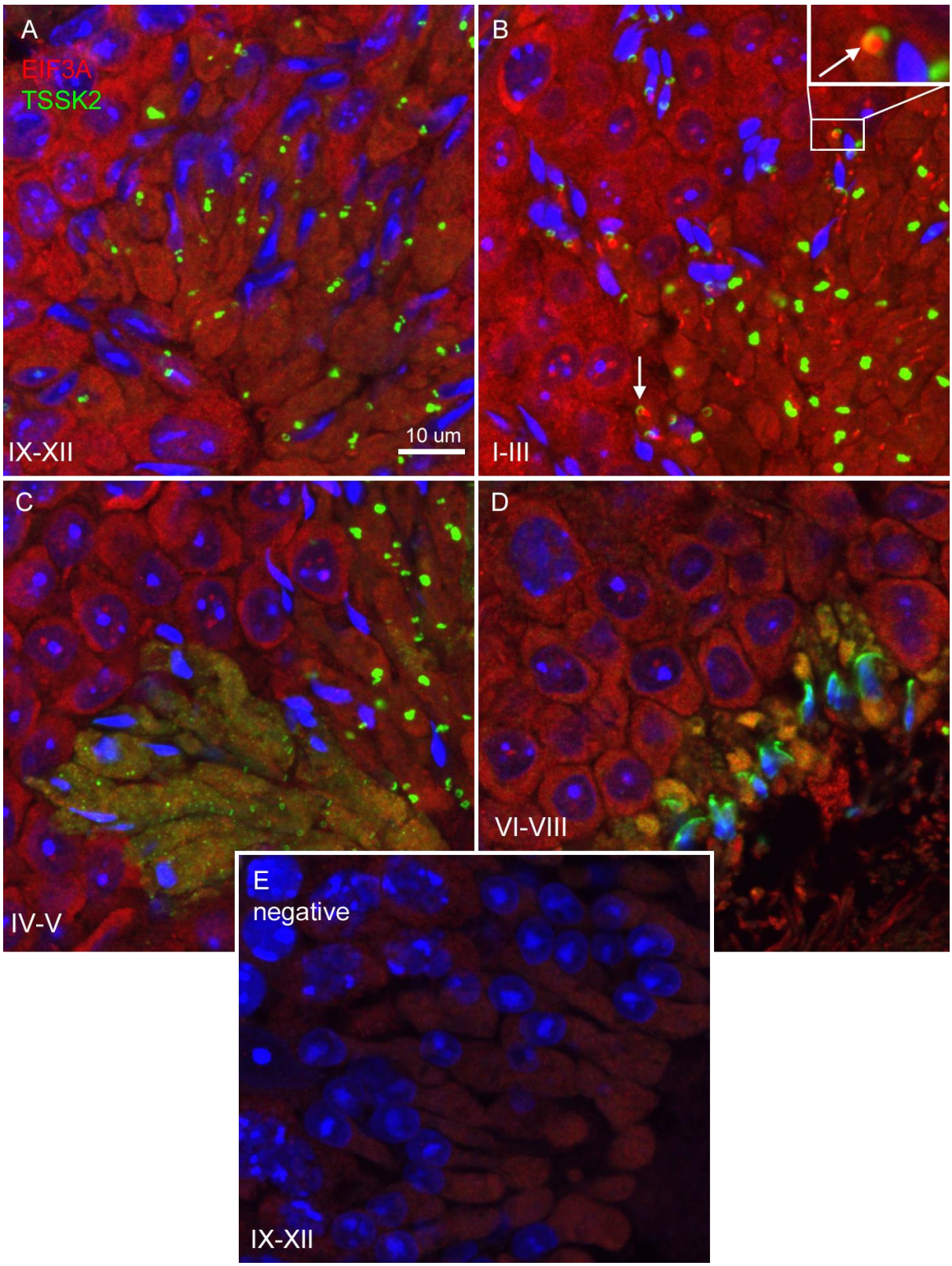

Figure 13. TSSK2 and eIF3F localization in WT mouse testis sections during different stages of spermatogenesis. A-D) TSSK2 (green) staining is detected in the same pattern as in previous stainings, from ring and satellite late CB in earlier elongating spermatids to diffuse staining in late elongating spermatids. eIF3f (red) staining is similar to that of eIF3a in that it is mostly dispersed, cytoplasmic and expressed in all cell types of the tubules, but with distinguishable concentrated areas of expression that sometimes overlap TSSK2. E) Negative control of stage VI-VIII for reference.

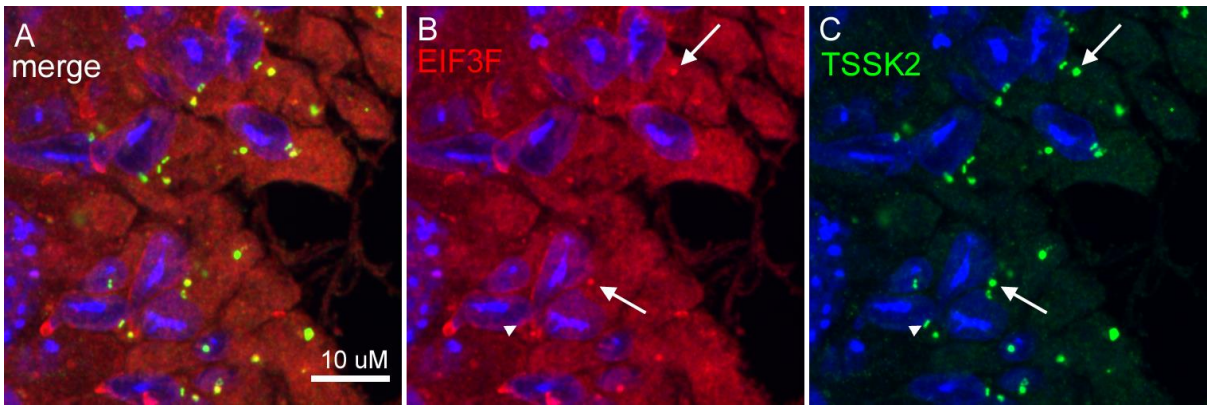

Figure 14. TSSK2 and eIF3f co-localize in stages IX-XII. Concentrated eIF3f (red) dots can be seen in elongating spermatids, appearing to co-localize with TSSK2 (green) stained late CB satellite structure (arrows). In some elongating spermatids, the ring structure (arrowhead) has slightly overlapping signal as well.

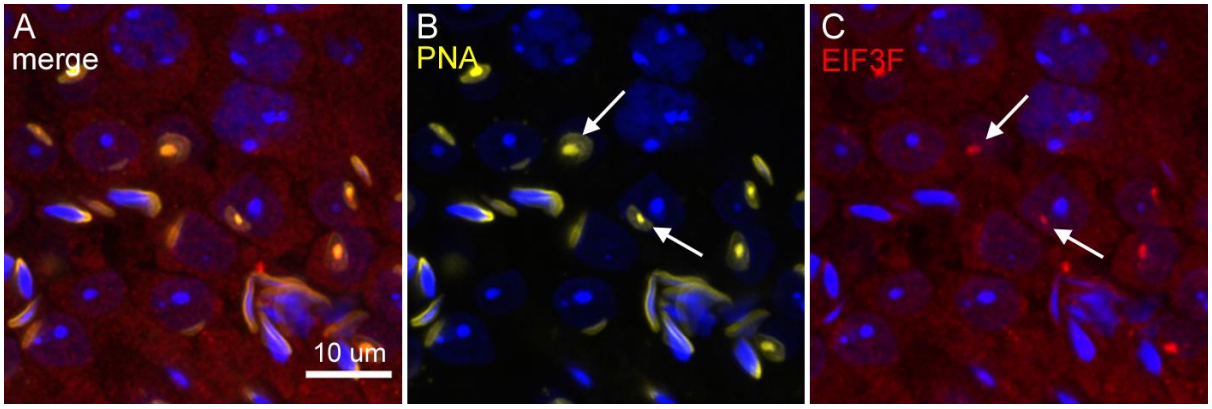

Figure 15. eIF3f co-localizes with acrosomal granule. When acrosomes are stained with PNA (yellow), eIF3f (red) can be seen in concentrated dots matching the acrosomal granules of round spermatids in stage II-V (arrows)

2.7 eIF3 and TSSK2 are closely associated in elongating spermatids

To visualize that eIF3 subunits and TSSK2 are in close contact with each other in elongating spermatids, a Duolink proximity ligation assay was used to detect proximity of these proteins in testis cross-sections (Figure 16). Duolink assay utilizes two types of oligonucleotide-linked secondary antibodies that target primary antibodies made in different animals, and when the two primary antibodies are closer than 40 nm apart from each other, the oligonucleotides can be enzymatically ligated to form a circle. The oligonucleotide circle can then be amplified with polymerase and detected with a fluorescent probe.

The assay was first tested with FYCO1, a protein that is known to localize to the CB and the late CB, to validate that the assay works in this application, as there are no previous

reports of Duolink proximity ligation assay being used on testis cross-sections. In Figure 16A, the green fluorescent signal detecting the close proximity between TSSK2 and FYCO1 can be seen in locations that accurately correspond to the expected sites of the late CB ring and satellite in elongating spermatids, as all signal is detected near the tubule lumen. The signal appears as specific dots, easily distinguished from small amounts of background fluorescence, and the signal is moderately present in all stages from I-III to IV-VIII and IX-XII. There is notably stronger green signal in the spermatid heads overlapping with the nuclear stain DAPI near the spermiation point.

Similar signal is detected in eIF3a and TSSK2 Duolink assay (Figure 16B) and in eIF3f and TSSK2 (Figure 16C). Signal in these two experiments was also almost completely luminal, located in elongating spermatid tails. eIF3a and TSSK2 assay had less nuclear green fluorescence in later step 16 elongating spermatids of stage IV-VIII, whereas in eIF3f and TSSK2 assay the staining was very prominent in these late step spermatids. There were differences in the background fluorescence as well, with eIF3f and TSSK2 assay having more green background fluorescence, which possibly explains the difference in step 16 spermatid nuclear staining. Negative controls were performed with all the antibodies alone, and no antibodies at all, to confirm the specificity of the assay (Figure 17). All the controls were empty. Here, the results of the Duolink proximity assay show that eIF3 complex is closely associated with TSSK2 in elongating spermatids.

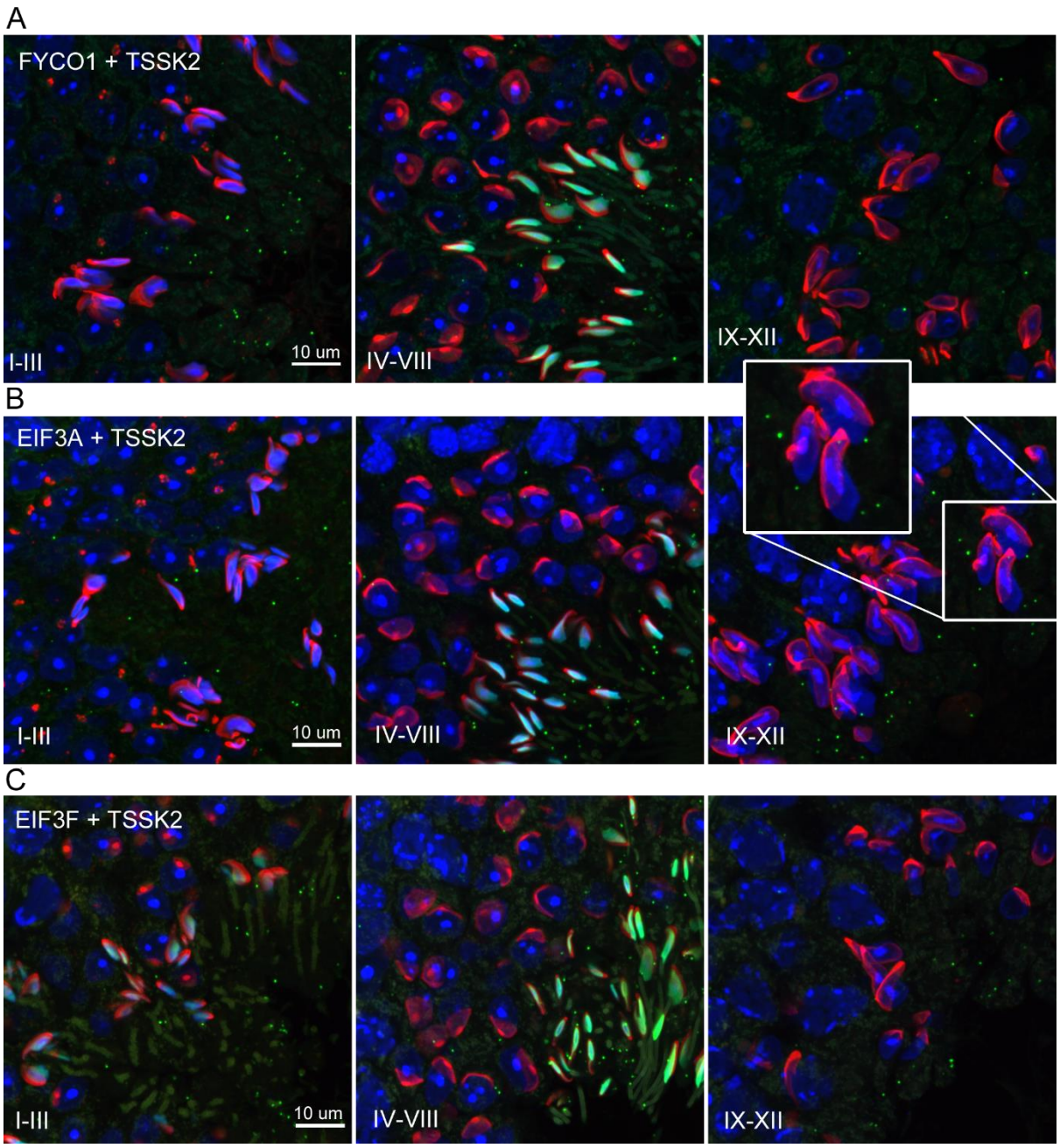

Figure 16. Duolink of TSSK2 with its interaction candidates eIF3a and eIF3f and a known late chromatoid body component FYCO1. The signal of the two antibodies being <40 nm apart from each other is detected via green fluorescence, and the results of each pair of antibodies in different stages is represented by a row in the figure. A) TSSK2 and FYCO1 are localizing near each other in different stages of spermatogenesis from I to XII as depicted by the green dots in the lumen of the seminiferous tubule. Signal is also seen in the head of the late step spermatids. B) TSSK2 and eIF3a. Duolink signal is seen in the lumen throughout stages I-XII. In the insert, arrowhead marks a site of interaction localizing near the neck of the elongating spermatid, where the late CB ring would be also located. C) TSSK2 and eIF3f. Duolink signal is seen in the lumen but also very prominently in the head of the late step spermatids.

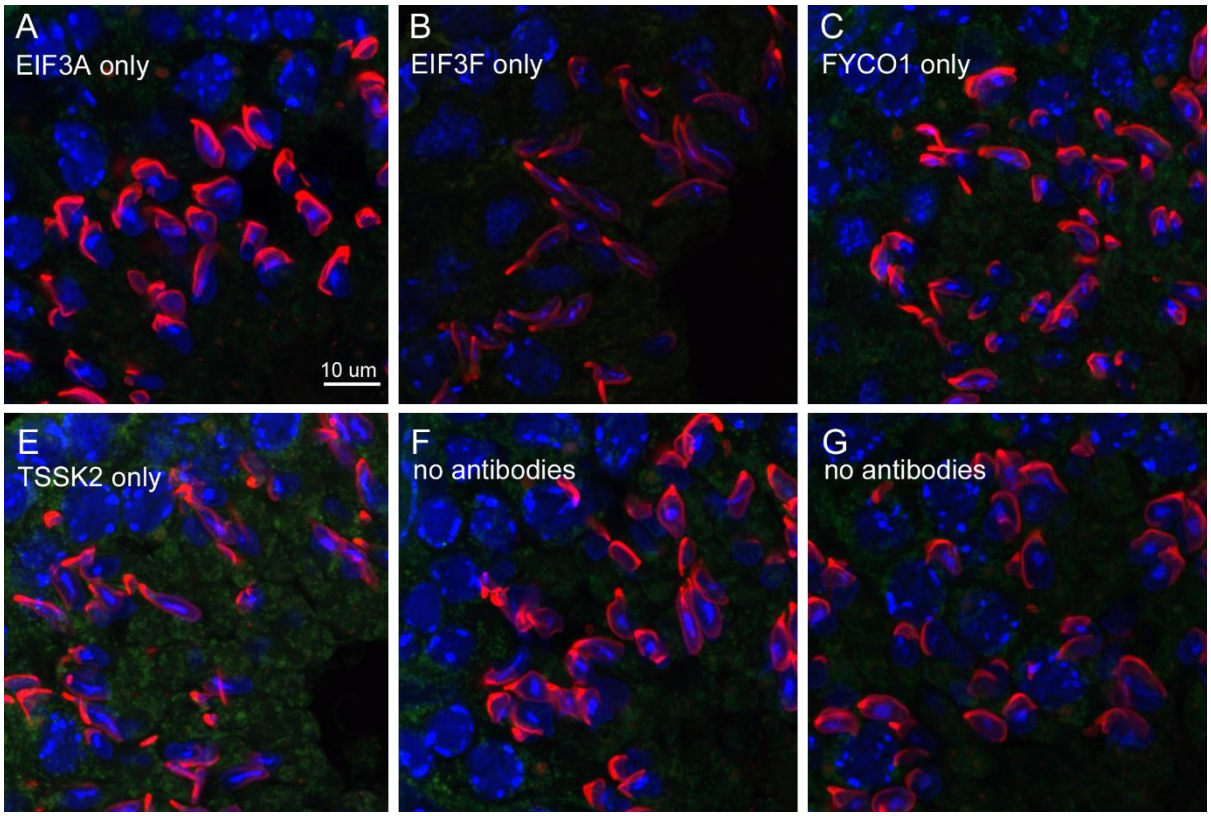

Figure 17. Negative controls for the Duolink assay. Negative controls with only one primary antibody, or no antibodies, were treated with the same conditions as the samples. TSSK2 gave some faint nonspecific diffuse background autofluorescence (d), but otherwise the controls were all empty.

2.8 The late CB is associated with translational activity

To examine nascent protein synthesis in elongating spermatids and to localize translational activity to the late CB, seminiferous tubule pieces were shortly cultured with a methionine surrogate L-azidohomoalanine (AHA), that would be incorporated in newly synthetized proteins. Tubule pieces were then squashed to slide and treated with fluorescent-labeled alkyne-containing probe that binds to the azido moiety of AHA via click chemistry, allowing its detection as green fluorescent signal. AHA click-staining was combined with TSSK2 immunofluorescence to detect any overlapping signal. DMSO and a combination of AHA and a known translational inhibitor cycloheximide (CHX) were used as negative controls for the experiment.

As figure 18 shows, most of the newly synthetized proteins reside in the cytoplasm of spermatocytes, round and elongating spermatids and other cell types of the tubule in a diffuse manner. However, occasionally some concentrated AHA staining in elongating spermatids was detected near the neck of the spermatid, parallel to the late CB structures

stained by TSSK2 (Figure 17A). This was seen in step 12-13 elongating spermatids, at stages XII-I. The concentrated AHA signal overlapped especially the satellite body but was also seen in very close proximity with the ring structure. In later step elongating spermatids of stages V-VIII, the concentration of AHA signal in the proximity of TSSK2 positive granules was less prominent (Figure 17B). Instead, the signal was uniform throughout the flagellum. DMSO control (Figure 17C) and CHX control (Figure 17D) had some faint background fluorescence but a clear difference to the AHA samples, verifying that the AHA staining was credible. Altogether, accumulation of AHA-labeled nascent proteins was detected in sites corresponding the late CB in step 12-13 elongating spermatids, suggesting a connection between the late CB and translational activity.

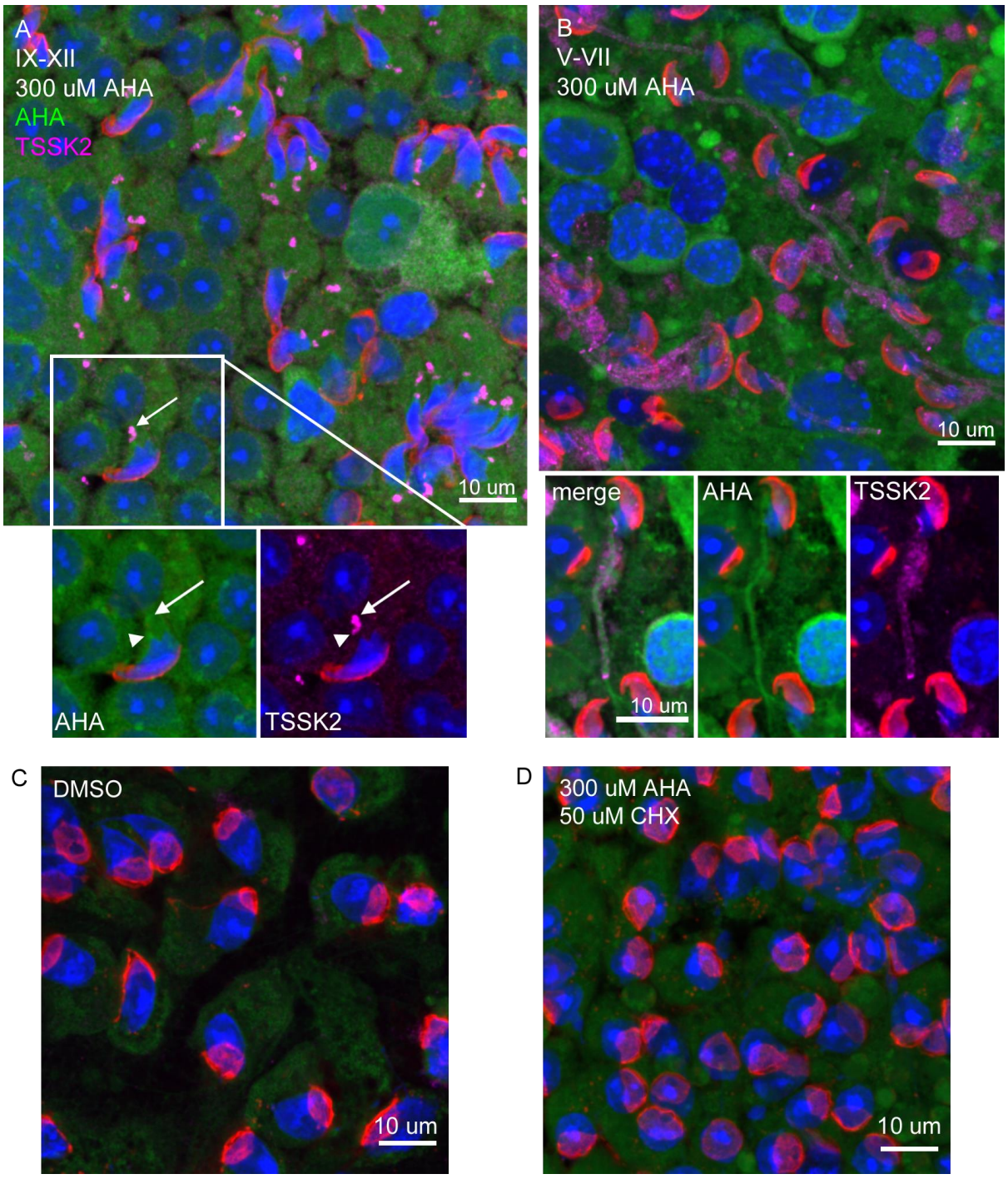

Figure 18. Translational analysis of germ cells with methionine surrogate AHA and Click-chemistry. A) A representative image of stage XII-I seminiferous tubule piece treated with 300 uM AHA (green), squashed to slide and stained with TSSK2 (magenta). The insert highlights a site where the late CB satellite body (arrow) and ring (arrowhead) are seen to overlap with concentrated AHA signal. B) Stage V-VIII tubule piece treated with 300 uM AHA. TSSK2 ring has migrated to the caudal end of the middle piece, and cytoplasmic TSSK2 staining is seen in the middle piece. AHA was not detected to concentrate in specific locations in these late step elongating spermatids. C) DMSO control had some low intensity green fluorescence background. D) Stage IX-XII tubule piece treated with 300 uM AHA and 50 uM CHX to inhibit translation. Background fluorescence of the sample was comparable to the DMSO control.

3. Discussion

Spermatogenesis is a highly complex cell differentiation programme that requires extensive post-transcriptional regulation. The transcriptome of the testis is enormous compared to any other tissue or organ, demonstrating the indisputable requirements for RNA regulatory mechanisms (Soumillon et al., 2013). This is most evident in the haploid male germ cells, of which especially the round spermatids have an exceptionally diverse transcriptome of ncRNAs in addition to protein coding RNAs (Soumillon et al., 2013). The CB has been long recognized as a pivotal organelle for RNA processing and metabolism in round spermatids, but after its transformation into the late CB in the beginning of spermatid elongation, its role has remained elusive. Herein, the aim of this study was to elucidate the late CB function in spermatogenesis and to study its newly discovered possible relation to translational control during spermatid elongation.

3.1 Examining the late CB protein composition

The first effort to investigate the late CB was to analyze its protein components. A few proteins have already been reported to localize in the late CB: TSKS, TSSK1, TSSK2, FYCO1 and GRTH/DDX25 (Gonadotropin-regulated testicular RNA helicase/ DEAD-box helicase 25) (Shang et al., 2010; Da Ros et al., 2017; Onohara and Yokota, 2012). However, their role in spermatid elongation is mostly unknown, except for TSSK1 and TSSK2, that have been shown to be essential for mitochondrial sheath formation and fertility in mice, as reported by Shang et al., 2010. Unlike TSKS, TSSK1 and TSSK2, that accumulate to the late CB after its transformation, FYCO1 and DDX25 are already present in the CB of round spermatids (Da Ros et al., 2017; Sato et al., 2010). FYCO1 has been shown to mediate CB-associated autophagy and lysosomal vesicle transport and is required for maintaining the integrity of the CB (Da Ros et al., 2017). DDX25 has been found to be associated with the CB by transporting mRNA transcripts from nucleus to the CB, and it has also been shown to be integral for the CB structural integrity (Sato et al., 2010). This leaves TSSK1, TSSK2 and TSKS as the only components that are specific to the late CB only, and therefore we were interested in these proteins as late CB markers for further studies on the late CB function. We found that TSSK2 has remarkable specificity for the late CB ring and satellite structures, which is in line with the previously published data (Shang et al., 2010). This made TSSK2 our protein of interest for co-immunoprecipitation and the following mass spectrometry analysis, to identify novel TSSK2 interaction candidate proteins.

The interesting new discovery from mass spectrometry was that a large amount of translation associated proteins was found to be linked with TSSK2, a finding that has not been reported previously. A trend of proteins involved in initiation of translation was especially prevalent, with eIF3 among the most abundant proteins of the analysis. Other translation initiation related proteins supported this connection, from 60S and 40S ribosomal subunit proteins to elongation factors alpha-1, delta and gamma that deliver tRNA to ribosomes (Negrutskii and El'skaya, 1998) and DEAD-box helicases 1 and 3x, that are involved in mRNA metabolism (Rocak and Linder, 2004). But as 11 out of 13 subunits of eIF3 were present in the analysis and the subunit eIF3a was one of the most abundant single peptides of the samples, this became the lead TSSK2-interaction candidate for further investigation.

3.2 Eukaryotic initiation factor 3

eIF3 is one the first identified, largest and most complex of the initiation factors involved in translation initiation (Hinnebusch, 2006). Translation in eukaryotic cells takes place in ribosomes that consist of two subunits, small 40S subunit and large 60S subunit. Translation initiation requires a coordination of at least 12 eukaryotic initiation factors to assemble the preinitiation complex (PIC). PIC is composed of the two ribosomal subunits, initiating methionyl tRNA and mRNA, and the involvement of eIFs in PIC is essential for accurate protein synthesis. Recognition of the correct mRNA start codon also relies on eIFs. (Jackson et al., 2010)

In translation initiation, eIF3 has been indicated to have a central role in organizing numerous initiation pathways (Hinnebusch, 2006). eIF3 functions range from facilitating the activity of other eIFs and recruiting PIC components to scanning mRNA for the AUG start codon. Mammalian eIF3 is composed of 13 subunits from eIF3a to eiF3m. Each subunit has their specific, essential function in the complex, with the exception of eIF3j, that binds only loosely on the complex and is mostly not required for effective translation initiation. Of all the eIF3 subunits, eIF3a and eIF3f were chosen for this project because of their abundance in the mass spectrometry analysis and because both of them have already been studied during spermatogenesis. eIF3a and eIF3f are both core subunits of the eIF3 complex, and they are also interacting partners to each other (Hinnebusch, 2006). The functions of eIF3a have been indicated to include recruiting the 40S ribosomal subunit and mRNA to the PIC, and binding eIF4b to promote eIF4s's RNA helicase activity (Hinnebusch, 2006). eIF3f has been linked with contradictory functions in translation

activation, but also in translation inhibition (Marchione et al., 2013). It is possible that both eIF3a and eIF3f have independent regulatory roles outside of translation initiation, a topic that will be shortly discussed next.

Considering the fundamentality of eIF3 in both somatic and germ cells in translation initiation, it could be speculated that it has a regulatory role during late spermatogenesis when transcription diminishes, and protein synthesis depends on the activation of translation of the existing, stored transcripts. Interestingly, eIF3 has been linked to translational control during earlier steps of spermatogenesis via interaction with the murine PIWI protein MIWI (Dai et al., 2019), and another PIWI protein MILI (Unhavaithaya et al., 2009). These reported associations include the subunits EIF3a and EIF3f. As MIWI and MILI are both known components of the CB, eIF3 seems to share an interaction with both the CB and the late CB.

3.3 Confirming the interaction between TSSK2 and eIF3 with co-IP

The suggested possibility of the late CB involvement in translation initiation caught our attention, but confirmatory studies of TSSK2 and eIF3 interaction needed to be performed first. Co-IPs with TSSK2 and eIF3a were performed to verify that TSSK2 would pull down eIF3a and eIF3a would pull down TSSK2. However, as the results show, we only managed to detect eIF3a in the TSSK2 IP but TSSK2 was not detected in the eIF3a IP. Many variables were optimized in the IP protocol, including duration and number of the IP washes, amount of testis lysate used as starting material, primary antibody dilutions, blotting conditions and washes of the immunoblotted membrane after primary and secondary antibody incubations. Despite the numerous attempts of optimization, some issues remained unsolved. For example, although clear eIF3a signal was detected in the eIF3a IP sample, as well as in the TSSK2 IP sample, the signal was not detected in the lysate input samples. This could be caused by the eIF3a IP samples binding to a significantly larger amount of target antigen compared to what was present in the fairly small amount of lysate sample loaded to SDS-PAGE. However, the protein content of the lysate was measured and normalized to 100 ug, which should be a sufficient amount of protein per well to be detected with western blotting. The reason why eIF3a was pulled down from TSSK2 but not vice versa is more puzzling, but this could be affected by the binding properties of the eIF3a antibody. In any case, the positive result from TSSK2 IP probed with eIF3a confirmed that TSSK2 and eIF3a associate in the mouse testis. One

option to truly confirm the interaction would be to perform mass spectrometry with eIF3a IP samples and demonstrate the presence of TSSK2 in the analysis.

3.4 Ontogeny of TSSK2 and eIF3a

The next step was to characterize TSSK2 and eIF3a association temporally and spatially in the testis. Western blotting with TSSK2 and eIF3a was performed in a series of testis samples from 1 to 5 week-old, 7 week-old and 10 week-old mouse testes. This revealed a differential expression pattern, as eIF3a was uniformly present from the very first week to young adulthood of the mice, but TSSK2 signal was not visible until week 5. The continuous expression of eIF3a in the developing testes was of course expected, as eIF3 is fundamental for translational activation in all cell types of the testis. The TSSK2 expression pattern that we observed is also supported by literature, as the start of the spermatid elongation takes place around the onset of puberty, in week 4 or week 5 in mice (Horowitz et al., 2005). The progress of spermatogenesis at that point is of course very fast, and to record the first appearance of TSSK2 accurately, more precise timepoints would have been needed for the samples. An intriguing notion about the eIF3a western blot was that the faint smaller bands around the size of 50 kD seemed to be more prominent from week 1 to 3, whereas the bands around 100 kD were more prominent from week 4 to 10. These could be just degradation products of eIF3a, but they could also be speculated to be some spermatogenesis specific isoforms. All in all, from week 5, TSSK2 and eIF3a were both confirmed to be present in the testis lysates.

3.5 Novel findings on the cellular localization of eIF3a and eIF3f in elongating spermatids

To characterize TSSK2 and eIF3 interaction in cellular level and more detail, immunofluorescence assays on testis cross-sections and isolated germ cell preparations of different stages were performed. Immunostainings confirmed that eIF3a and eIF3f were both expressed in elongating spermatids and their localizations were associated with the late CB structures, but at different stages of spermatogenesis. eIF3f was found to localize in earlier step elongating spermatids during stages IX-XII. This speculated co-localization took place very prominently in the late CB satellite, but the ring structure had some overlapping eIF3f staining as well. In contrast, eIF3a was not found to have any concentrated signal in elongating spermatids until stages I-III, where eIF3a was seen to be expressed in curious, strand-like patterns that extended towards tubule lumen from

elongating spermatids. Here the late CB corresponding localization sites of eIF3a were seen in the ring but not necessarily in the satellite. As little as is currently known about the late CB in spermatogenesis, even less is known about the possible independent roles of the ring and the satellite, but these findings suggest that they are both somehow involved in translation initiation by their association with different eIF3 subunits. Besides these more concentrated localization sites, it is to be noted that the eIF3-TSSK2 interaction demonstrated with the co-IP and mass spectrometry could also be cytoplasmic. TSSK2 is not wholly specific to the late CB but is also found in the cytoplasm of elongating spermatids. In the immunofluorescence assays, this cytoplasmic TSSK2 is seen especially in stages V-VIII, and in the very late step 16 elongating spermatids of stage VII and VIII just before spermiation, TSSK2 is also seen to accumulate in the acrosome. Interestingly, with eIF3f immunofluorescence we found that eIF3f co-localizes with the acrosomal PNA staining, and hence it could be speculated that some TSSK2 and eIF3f interaction could take place in the acrosome as well.

3.6 Proximity assay reveals nearby localization of TSSK2 and eIF3 subunits

To further study the proximity of eIF3 and TSSK2 in elongating spermatids, a Duolink proximity ligation assay was performed. Our approach was to perform the assay in testis cross-sections, with primary antibody incubations similar to the immunofluorescence assays, but proceeding with the Duolink technique. Proximity ligation assay involves specific secondary antibodies to recognize primary antibodies made in different animals, and when two of the primary antibodies are closer than 40 nm apart from each other, they are enzymatically ligated with oligonucleotides, that in turn can be polymerized and probed with a fluorescent label (Gustafsdottir et al., 2005).

This assay has not been reportedly used in testis cross-sections before, which is why FYCO1, a known late CB component, was used with TSSK2 to validate the assay. The results of FYCO1, eIF3a and eIF3f paired with TSSK2 were all similar, with empty controls and Duolink signal detected in the elongating spermatids near tubule lumen throughout spermatogenesis. Herein, we also report successful application of the assay in testis cross-sections. However, not all antibodies that we tried in the Duolink assay together with TSSK2 provided such solid results. The eIF3a antibody that was originally used for western blotting, co-IP and the immunofluorescence assays, gave indistinguishable signal in both the actual assay with TSSK2 and the control that was treated with eIF3a only.

Therefore, another antibody against eIF3a from Sigma-Aldrich was used in Duolink instead to obtain better results.

Overall, the results of the proximity ligation assay have their limitations. The assay does not show where the proximal localization is taking place in an elongating spermatids. Some structural components of the elongating spermatids could have been visualized with additional immunostaining after the Duolink protocol, but the antibody would have required to be made in a different animal than the antibodies used in the Duolink assay itself, and such an antibody was not available for us. Instead, in an effort to detect more precise locational information on the proximal location sites in elongating spermatids, the proximity ligation assay was tried on isolated germ cell preparations. This did not work however, as negative controls with single antibody alone gave too much signal to make any conclusions from the actual samples.

Nevertheless, the Duolink proximity ligation assay confirmed that a nearby localization of <40 nm between FYCO1 and TSSK2, eIF3a and TSSK2, and eIF3f and TSSK2 is present in the elongating spermatids. An interesting Duolink signal was detected also in step 16 spermatid heads during stages V-VIII. The localization of TSSK2 in acrosomes of step 16 elongating spermatids in immunofluorescence, and the fact that this staining was not seen in any of the controls supports that the signal could be true, and there is in fact some nearby localization of the examined proteins in step 16 elongating spermatid heads. On the other hand, the staining seems to be more nuclear than acrosomal, which is contrary to what is seen in TSSK2 or eIF3a or eIF3f immunofluorescence, and the signal also differs greatly from what is seen in the tail regions of elongating spermatids. The intensity difference could be explained by an increased number of the studied proteins localizing near each other in the head, but again, this is not very strongly supported by our previous findings. For now, this question remains unanswered.

3.7 Active protein synthesis takes place adjacent to the late CB

After a sufficient amount of evidence was obtained to support the hypothesized interaction between TSSK2 and eIF3, we tested the second hypothesis of the late CB involvement in translation initiation in elongating spermatids. For this purpose, seminiferous tubules were cut in stage specific pieces and shortly cultured in a methionine-free medium containing a non-canonical amino acid AHA that is analogous to methionine. In absence of methionine, AHA replaces it in all freshly synthesized proteins of the cultured tubules. Using a click reaction, the azido moiety of AHA can be linked with alkyne-containing fluorescent label to

visualize the nascent proteins (Hein et al., 2008). Combining this method with TSSK2 immunofluorescence staining, we were able to investigate the translational activity of elongating spermatids, locate the translationally active sites and compare them to the TSSK2 stained late CB structures. The results showed that there are translationally active foci in step 12 or 13 elongating spermatids of stage XII-I that in some instances overlap with TSSK2 signal. This overlapping was located to the neck area of the elongating spermatids, where it seemed to at least partially match both the satellite and ring late CB structures stained with TSSK2. This is in line with the localization patterns seen in the TSSK2 and EIF3a immunofluorescence assay of testis cross-sections, where they localized near each other in the neck of the step 13 spermatids at stage I. In later step elongating spermatids of stage V-VIII, the translationally active foci were no longer detected. This, along with the results from both immunofluorescence assays of EIF3a and EIF3f with TSSK2, suggests that the association of TSSK2 or the late CB and protein translation is temporary and subsides as spermatid elongation proceeds to steps 15 and 16. To make sure that the AHA staining was true, negative controls were performed with two different methods. The first control was incubated with DMSO only, to rule out that the DMSO would affect the assay, as it was the diluent used in the AHA reagent. The second control was incubated with 300 uM AHA with 50 uM CHX to inhibit protein synthesis. Although both controls had some faint background fluorescence, it was significantly lower than in the AHA samples.

All experimental conditions for AHA analysis required a lot of optimization before acquiring reliable results. One of the biggest challenges with this experiment was the short-lived seminiferous tubule culture. As tubule pieces are removed from their physiological environment in mouse testis, the cells are put under a lot of stress. This may alter the protein synthesis and AHA incorporation into newly synthesized proteins, or lead to cell death, both negatively affecting the results and validity of the experiment. For this reason, the experiment had to be performed in a very fast pace from dissection of the testes to cutting the tubule pieces and setting up the culture with different experimental conditions. However, cutting the tubules requires precision to obtain tubule pieces of the desired stages, and similar in size to ensure even AHA incorporation into them. This inevitably takes some time. After cutting the tubule segments, the incubation time had to be optimized. It needed to be short enough for the cells to remain in good shape, but long enough for a detectable number of proteins to get synthetized with AHA incorporated in them. The AHA and CHX concentrations needed some titration as well, as most of the

AHA analyses reported in literature have been performed with more traditional cell cultures and were not translatable to our experiment. The concentrations were gradually increased in different experiments to use the reagents sparingly, and to make sure that CHX concentrations were not high enough to cause any toxic effects on the cells. After the tubules were treated with either DMSO, AHA, or AHA and CHX, they were squashed and fixed to a slide. Squashing is a simple technique to spread the germ cells from the tubule to the slide, but it also presents its own challenges. The length and shape of the tubule, how delicately the coverslip is placed on top of it, and how successfully the cells are spread after placing the coverslip can all affect the outcome. Especially air bubbles under the coverslip can obstruct the cells from spreading properly. As squashing takes some time for each sample and there were plenty of samples to be squashed in each experiment, there is also some variability in the actual incubation times of the tubules from 45 minutes forward. This may affect the final results when comparing samples that were squashed first versus the samples that were squashed last. Finally, the fixation of the samples needed some optimization to try and reduce unwanted background fluorescence. This was present especially in the first few attempts of the AHA assay. The five minute fixation after squashing was tried with 96% ethanol, 100% methanol and 100% acetone but, there was no significant difference observed between these three, so we continued with ethanol fixation. The post-fixing with 4% paraformaldehyde was first tried straight after the ethanol fixing, and then with a few additional PBS washes before the post-fixing. As neither of these methods provided good results, the ethanol fixed slides were then left to dry O/N to perform post-fixing and click-it reaction the next day, and this method appeared to work the best. After all this optimization, we could obtain the anticipated results with low signal controls and distinguishable AHA signal in samples. Some variability remains between different samples due to complexity of the assay, but altogether we successfully established an assay to investigate active translation in a male germ cells and utilized it to support the hypothesis that the late CB is connected with translation.

3.8 The possible role of late CB in RNA regulation

The connection of the late CB with eIF3 and translation initiation thereby suggests that the late CB is involved in RNA regulation of elongating spermatids. Considering its predecessor's, the CB's role in RNA regulatory processes of round spermatids, it would be logical for the late CB to retain some functional similarity with the CB in this regard. Germ granules are predominantly characterized by their RNA regulatory functions, from the processing bodies or piP-bodies to IMC and the CB (Voronina et al., 2011). For example,

IMC of spermatogonia and spermatocytes shares many piRNA pathway-associated proteins such as MILI and MIWI2 with its successor, the CB (Meikar et al., 2011). However, it is not self-evident that germ granules should be limited to this function. The CB has been found to contain aggresomal pathway proteins that are involved in degradation processes of DNA, RNA and proteins (Haraguchi et al., 2005). Furthermore, the late CB lacks the piRNA-pathway proteins and instead it has a role in cytodifferentiation of the elongating spermatid middle piece and mitochondrial sheath (Shang et al., 2010).

The late CB and TSSK2 are hence demonstrated to exert functions in both RNA regulation and the assembly of mitochondria in elongating spermatids. These two functions may well be related. TSSK2 and the late CB might mediate translation or post-transcriptional modification of proteins that are involved in mitochondrial sheath formation. During later steps of spermiogenesis, when the transcription ceases, the role of eIF3 in activation of translation of such proteins ought to be pronounced. As cytodifferentiation of the sperm tail, including the mitochondrial sheath formation, is a complex process involving a diversity of proteins, it likely requires highly precise control mechanisms. Thereby, considering the association between TSSK2 and eIF3 that we found, it could be speculated that the late CB coordinates the activation of protein synthesis during spermatid elongation. For instance, the late CB could release stored mRNA for translation, that is then initiated by eIF3.

The association with tail differentiation would seem likely especially for the late CB ring, as it first locates to the neck of the spermatid, but then migrates in front of the mitochondrial sheath to the caudal end of the middle piece. The cytoplasmic localization of the late CB satellite in turn might suggest that it is involved in more cytoplasmic regulatory processes. However, as described earlier, there is also a possibility that TSSK2 and eIF3 interplay takes place in the cytoplasm and not the late CB.

3.9 Strengths and limitations of this study

In fact, the inability to distinguish between cytoplasmic, late CB ring-associated and late CB satellite-associated TSSK2 is one of the major limitations of this study. This challenge is present from the first TSSK2 co-IP and mass spectrometry results to the experiments confirming the TSSK2 and eIF3 interaction. However, the immunofluorescence assays provide proof that some level of interaction takes place in both the ring and the satellite structures, with eIF3a and eIF3f, respectively. The translationally active foci in the AHA assay would also suggest that translational regulation is not solely diffuse and cytoplasmic,

but instead somewhat concentrated in a late CB associated manner. Still, this issue needs further investigating. One approach to examine more specifically the late CB composition would be to immunoprecipitate it as a whole organelle. For this purpose, a chromatoid body isolation protocol could be applied and modified, introducing the cross-linking to preserve more protein-protein interactions, but using TSSK2 for immunoprecipitation. One approach to study TSSK2 involvement in translational control would be to isolate ribosomes by polysome profiling and to investigate if TSSK2 is present in the polysome fraction of a testis lysate.

A question concerning the mass spectrometry results was the absence of FYCO1 and DDX25. FYCO1 has been shown to be connected with TSSK2 and the late CB with previous mass spectrometry analysis of TSSK2 co-IP (Shang, 2014), whereas DDX25 has been shown to co-localize with the late CB in immunofluorescence assays(Onohara and Yokota, 2012). The lack of these proteins in the mass spectrometry analysis could be caused by a limited sensitivity of the co-IP, perhaps due to low affinity binding or very rapid dissolution of the interacting proteins. The quality of the testis lysates and protein degradation could also partially explain this issue.

Some issues that were faced in this study were related to the performance of the antibodies that were used. For example, the original eIF3a antibody did not work properly in Duolink and therefore another eIF3a antibody from different producer was used. eIF3f antibody worked well in immunofluorescence and Duolink, but not in WB or co-IP. However, it is typical for antibodies to work better in some applications than in others. Apart from these instances, using antibodies against two different eIF3 subunits to characterize eIF3 and TSSK2 connection is one of the strengths of this study. Proper controls were employed in each experiment to validate the results, and all of the experiments were performed multiple times to confirm the reproducibility of the results.

3.10 Significance of the results

Although future studies are needed to further examine the interaction, ultimately, we have revealed eIF3 complex as a novel interaction candidate to TSSK2 and explored the connection between the late CB and translation. This is important information in elucidating the complex factors affecting spermatogenesis and male fertility, as TSSK2 depletion in the TSSK1/2$^{-/-}$ KO model is shown to cause male infertility in mice (Shang et al., 2010). Another study found that in induced-oligoasthenospermia mouse model, TSSK2 protein and mRNA expression was decreased (Zhang et al., 2020). In humans, single-

nucleotide polymorphisms (SNP) in TSSK2 have been indicated to be associated with azoospermia and severe oligospermia (Salicioni et al., 2020). These are both pathologies leading to male infertility: azoospermia, a condition where no sperm is found in the semen, affects approximately 1% of males and is found in 10-15% of infertile males (Cocuzza et al., 2013). In severe oligospermia, the sperm count of semen is drastically decreased. According to one meta-analysis, male infertility was found to affect around 30 million males worldwide, contributing to approximately 50% of infertility cases of couples (Agarwal et al., 2015). As 15% of couples worldwide suffer from infertility, this a very relevant and active field of research. Understanding the molecular factors and processes behind male reproductive pathologies may aid in developing new diagnostics and treatments.

While in some instances infertility is a medical and humanitarian problem, in other instances it may be in fact a desirable outcome. The prevalence of unintended pregnancies is high, estimated to be around 40% worldwide (Singh et al., 2010). This demonstrates a clear unmet medical need for new contraceptive strategies. TSSK1 and TSSK2 have already attracted interest as targets for non-hormonal male contraceptive development (Salicioni et al., 2020). Some advantages of TSSK1/2 as male contraceptive targets include their specificity to late step spermatids of testis, which suggests that any unwanted or systemic effects would be unlikely and the effect on fertility would be reversible. They also belong in a specific family of kinases, which enables the development of small molecule kinase inhibitors with good specificity for the target, high efficiency and oral administration route. However, the precise mechanism of action by which TSSK1/2 inhibition leads to infertility is not discovered yet. Therefore, this study provides utmost important information on TSSK2 as a drug target as well.

3.11 Conclusion

In conclusion, this study has revealed a previously unknown interaction between TSSK2 and eIF3 in the late CB during spermatid elongation. The presence of eIF3 complex and the accumulation of AHA-labeled nascent proteins in the late CB support the hypothesis that the late CB function is connected to translation and RNA regulation of male germ cells. Relating these findings to a broader function of the late CB requires further studies, and the importance of TSSK2 and eIF3 interplay for spermatid elongation remains unknown. However, this study provides novel important information on the factors involved in the regulation of spermatogenesis that can be relevant to both physiology and pathology of male reproduction.

4. Materials and methods

4.1 Materials

4.1.1 Animals

The experimental animal models used in this study were adult WT male mice of C57BL/6Ncrl strain, obtained from Central Animal Laboratory of the University of Turku. The housing, handling and usage of experimental animals in this study is approved by the Committee on the Ethics of Animal Experimentation at the University of Turku, in accordance with the Guide for Care and Use of Laboratory Animals (National Academy of Science) (license number: 2009-1206-Kotaja).

4.1.2 Antibodies

Antibodies that were used are listed here: mouse monoclonal anti-TSSK2 (cat# H00023617-M01, Abnova/Novus Biologicals, USA), rabbit polyclonal eIF3a (cat# BT-E1F0D7, Nordic BioSite AB, Täby, Sweden), rabbit polyclonal eIF3a (cat# HPA038315, Sigma-Aldrich, Saint Louis, USA), rabbit polyclonal eIF3f (cat#AP2900a, Abcepta, San Diego, USA) and FYCO1 (cat# A96844, Atlas Antibodies, Bromma, Sweden). Secondary antibodies used in this study were anti-mouse AlexaFluor 488, anti-rabbit AlexaFluor 546 and anti-rabbit AlexaFluor 647 (cat# A21202, cat# A10040, cat# A31573, respectively, by Thermo Fisher Scientific, Massachusetts, USA). Mouse IgG (cat# NC-748-P, NeoMarkers, Fremont, USA) and rabbit IgG (cat# NC-100-P1, NeoMarkers, Fremont, USA) were used for negative control in immunoprecipitation. Glyceraldehyde 3-phosphate dehydrogenase (GAPDH) (cat# 5G4, HyTest, Turku, Finland) was used as a loading control for western blotting.

4.2 Co-immunoprecipitation and western blotting

4.2.1 Lysate preparation

For lysate preparation, testes were collected in ice cold lysis buffer (1%Triton X-100 (Triton) in sterile filtered phosphate buffered saline (PBS), 5 mM ethylenediaminetetraacetic acid (EDTA), 0.2 mM phenylmethylsulphonyl fluoride (PMSF), 1 x protein inhibitor cocktail (PIC), pH 7.4), in volume of 1 mL per testis, and lysed with a dounce homogenizer. Lysates were incubated on ice for 30 min and centrifuged for 20 min

with 13 000 rpm at +4 °C. Pellets were discarded and supernatants collected and stored at -20 °C.

For ontogeny analysis, testis lysates were made from testes that were frozen and stored at -80 °C (2-, 3-, 5-, 7- and 12-week old mouse testes) or freshly collected (1- and 4-week old mouse testes). The testes were suspended in ice-cold RIPA buffer (50 mM Tris-HCl (pH 8.0), 1% Triton, 0.5 w/v-% sodium deoxycholate, 0.05 w/v-% SDS, 1 mM EDTA, 150 mM NaCl) with protease inhibitors (0.2 mM PMSF, 1 mM DTT, 1 x PIC), using 100 uL of lysis buffer per 10 mg of tissue. The testes were then lysed with Qiagen TissueLyser with 50 oscillations/second for 2 min. After lysing the tissues, lysates were left on ice for 30 min, centrifuged 20 min with 13 000 rpm at +4 °C and supernatant stored at -20 °C until further use.

Upon use, testis lysates were thawed on ice and centrifuged 10 min with 13 000 rpm at +4 °C. To normalize the amount of protein to 100 ug per well in western blotting, and to ensure sufficient protein content in the co-immunoprecipitation (co-IP) samples, the protein content of the lysates was measured using the Pierce™ BCA Protein Assay (Thermo Fisher Scientific). The measurement was performed with Victor X4 plate reader (Perkin Elmer), and the protein concentration was calculated from a bovine serum albumin (BSA) standard series.

4.2.2 Co-immunoprecipitation

Co-immunoprecipitation was performed with magnetic Protein G Dynabeads (Thermo Fisher Scientific). One testis was used for one co-IP sample and two samples were always made parallel, one of the target antigen and one for negative control. Before immunoprecipitation, the lysates were precleared for 30 min at +4 °C with 15 uL of Dynabeads per two testes. 15 uL of Dynabeads was also used for coupling the antibodies TSSK2, eIF3a (Nordic BioSite), mouse IgG for negative control of TSSK2 and rabbit IgG for negative control of eIF3a. 5 ug of each antibody was used for the 15 uL of beads, and the antibody-Dynabead complexes were incubated 1 h at RT and washed twice with 0.1% Tween-PBS before proceeding with the co-IP. A magnet was used for securing the beads during the washes. The precleared lysate was then pooled together and divided equally between the antibody-coupled beads for an O/N incubation at +4 °C. A 30 uL sample of the precleared lysate was taken as the positive control for western blotting and stored at -20 °C. The following day, the co-IP beads were washed 3 x 5 min with ice cold 1% Triton-PBS at +4 °C. After the final wash and removing the remaining wash buffer, beads of each

co-IP sample were resuspended into 30 uL of 1% Triton-PBS for SDS-PAGE (sodium dodecyl sulphate polyacrylamide gel electrophoresis) sample preparation.

4.2.3 SDS-PAGE, silver staining and protein transfer

For SDS-PAGE, 10 uL of 4 x SDS sample buffer (0.2 M Tris-HCl, 0.4 M dithiothreitol (DTT), 8.0 w/v-% SDS, 6 mM bromophenol blue, 4.3 M glycerol) was added to 30 uL of sample. The samples were heated for 5 min at +95 °C before loading to the gels. Two different gels were cast based on the molecular weight of the target protein: 10% SDS-polyacrylamide gel for TSSK2 (39 kD) immunoblotting and 7% SDS-polyacrylamide gel for eIF3a (167 kD) immunoblotting. 20 uL of sample was loaded per well and the SDS-PAGE was run with 15 mA per gel until the proteins were properly resolved. Proteins were then transferred to PVDF membranes with wet transfer using cold Towbin buffer (25 mM Tris-HCl, 192 mM glycine, 20% methanol, pH 8.3) for 1 h with 100 V constant. After protein transfer, silver staining of the TSSK2 co-IP gel was performed with Pierce Silver Stain Kit (Thermo Fisher Scientific) following the manufacturer's instructions

4.2.4 Immunoblotting

After protein transfer to PVDF, the membranes were blocked 1 h at RT with 5% milk in 1% Triton-Tris buffered saline (TBS). Primary antibody incubation was performed overnight at +4 °C with 1:1000 TSSK2 for the 10% SDS-PAGE resolved membranes and 1:500 eIF3a for the 7% SDS-PAGE resolved membranes, antibodies diluted in 1% milk in 1% Triton-TBS. Secondary antibody incubation was performed with 1:5000 horseradish peroxidase-conjugated anti-mouse or anti-rabbit IgG in 1% milk 1%Triton-TBS for 1 h at RT. The membranes were developed using Western Lightning™ ECL Pro kit (Perkin Elmer) and imaged with Sapphire Biomolecular Imager (Azure Biosystems).

To obtain a loading control for the ontogeny analysis, the membranes were dried, reactivated with 100% MeOH and stripped 2 min with stripping buffer (800 mM glycine, 1 w/v-% SDS, pH 2.5). 30 min blocking with 5% milk in 0.1% Triton-TBS followed, and primary incubation with 1:5000 GAPDH in 1% milk in 0.1% Triton-TBS was performed O/N at +4 °C. The washes, secondary antibody incubations and developing was done as described in the previous paragraph.

4.2.5 Mass spectrometry

Duplicates of both TSSK2 co-IP and mouse IgG co-IP samples made from different mice were sent to mass spectrometry analysis. Mass spectrometry was performed in the Turku Proteomics Facility, University of Turku and Åbo Akademi University. The facility is supported by Biocenter Finland. The data was processed by removing all hits that were found from mouse IgG co-IP samples, and the hits that were present in only one of the TSSK2 co-IP samples. After this, data was analyzed by sorting the hits according to coverage and/or number of peptides to find the most relevant interaction candidate proteins of TSSK2.

4.3 Immunofluorescence

4.3.1 Testis cross-sections

Testis cross-sections were cut from paraformaldehyde (PFA) fixed testes embedded in paraffin blocks with a microtome. The cross-section slides were dried O/N at +37 °C and stored at -20 °C. Upon use, slides were deparaffinized and rehydrated with xylene and alcohol series as follows: 3 x 10 min xylene, 2 x 10 min 100% ethanol, 2 x 5 min 96% ethanol, 2 x 5 min 70% ethanol and 2 x 2 min MQ-water. Antigen retrieval was performed in a pressure cooker for 2 hours in citrate buffer (100 mM, pH 6.0) or Tris-EDTA buffer (TE-buffer, 10mM Tris-HCl, 1 mM EDTA, pH 9.0). After this, slides were washed 4 x 3 min MQ-water and 3 min PBS. Blocking was performed with 10% normal donkey serum (NDS) and 3% BSA in PBS for 1 h at RT. Primary antibody incubations were overnight at +4 °C using the following dilutions: 1:1000 TSSK2, 1:200 eIF3a (Nordic BioSite), 1:300 eIF3a (Sigma-Aldrich) and 1:100 eIF3F, diluted in 3% NDS and 1% BSA in PBS. Negative controls were incubated with 3% NDS and 1% BSA in PBS without primary antibodies. 3 x 5 min 1% Tween20 (Tween)-PBS washes followed before 1 h incubation with 1:5000 rhodamine-conjugated peanut agglutinin (PNA, cat# RL-1072, Vector laboratories Inc, Burlingame, CA) for acrosomal stain and 1:500 anti-mouse AlexaFluor 488 and 1:500 anti-rabbit AlexaFluor 647 as secondary antibodies, all diluted in 3% NDS and 1% BSA in PBS. The incubation was carried out at RT, in a dark humified chamber, and all steps from hereafter were performed in dark to prevent photobleaching of the fluorescent secondary antibodies. The secondary antibody incubation was followed by 3 x 1% Tween-PBS washes and 10 min incubation with 1:10 000 DAPI (4′,6-diamidino-2-phenylindole) in PBS. A 5 min PBS wash and a quick rinse in MQ-water were performed before mounting. Finally, the slides were mounted with ProLong Diamond Antifade mounting medium (Thermo Fisher Scientific) with DAPI.

4.3.2 Drying down preparations

Mouse testes were collected and decapsulated in PBS. To obtain stage-specific germ cell preparations from seminiferous tubules, a protocol described by Kotaja et al.(Kotaja et al., 2004) was used. The method relies on the different light absorbance patterns of each stage of spermatogenic wave that can be observed under a transilluminating dissection microscope. Seminiferous tubule pieces can then be cut in specific stages corresponding to the transillumination properties, with stages IX-XII (right after spermiation) being almost transparent, and tubule gradually getting darker through stages I-V, until it reaches the dark zone at stages VI-VIII, where chromatin is fully condensed in late spermatids.

After cutting seminiferous tubule pieces of stages IX-XII, I-V and V-VIII, four pieces of each stage were transferred to a droplet of 100 mM sucrose solution on a petri dish. The tubules were minced with fine forceps and a germ cell suspension was made by gently pipetting the solution. 5 ul of the cell suspension was then added to 10 ul of fixing solution (1% PFA and 0.15% Triton in PBS, pH 9.0) on Superfrost Plus slides and left to settle O/N at RT in a dark, humified chamber. The following day, the slides were dried down at RT, washed 2 x 10 min with 0.1% Triton-PBS and air dried at RT again. Next, the slides were post-fixed with 4% PFA for 5 min and washed 3 x 5 min in PBS. Background autofluorescence was quenched with a 2 min incubation in 100 mM NH_4Cl, a 5 min PBS wash followed, and then the cells were permeabilized with a 5 min incubation in 0.2% Triton-PBS. 3 x 5 min washes with PBS followed before blocking with 10% BSA in PBS for 1 h at RT. Primary antibody incubation was performed overnight at +4 °C with 1:500 TSSK2 diluted in 3% BSA in PBS. Negative controls were incubated with 3% BSA in PBS without primary antibody. The next day, slides were washed 3 x 5 min in 0.1% Tween-PBS, and secondary antibody incubation was performed with 1:500 anti-mouse AlexaFluor 488 and 1:5000 PNA diluted in 3% BSA in PBS for 1 h at RT in a dark, humified chamber. All steps from hereafter were performed in dark. 3 x 5 min washes with 0.1% Tween-PBS followed, then a 10 min incubation with 1:10 000 DAPI and finally a 5 min PBS wash before mounting with Prolong Diamond Antifade with DAPI.

4.3.3 Imaging

Immunofluorescence stained slides were imaged with 3i Spinning Disk confocal microscope with 63x oil lens and stack imaging. In each experiment, the number of planes in the stack and the exposure time of each channel were kept uniform between different samples and the controls. Processing of the images was done with Image J/Fiji(Schindelin

et al., 2012), using maximum intensity z-projection and adjusting the channel intensities with uniform settings in all images of the same experiment.

4.4 Duolink proximity ligation assay

Duolink proximity ligation assay (PLA) was performed in mouse testis cross-sections to examine and confirm the nearby localization of TSSK2 and eIF3a on a cellular level. Testis slides were rehydrated and deparaffinized 3 x 5 min in xylene, 2 x 10 min 100% ethanol, 2 x 10 min 96% ethanol and 2 x 10 min 70% ethanol, and then rinsed 2 x 2 min with MQ-water. Antigen retrieval was performed by pressure cooking in TE-buffer for 2 h. A blocking solution provided by the Duolink kit was used for blocking 30 min at +37 °C in a pre-warmed humified chamber. Primary antibody incubations were performed overnight at +4 °C with the following antibody dilutions: 1:1000 TSSK2 combined with 1:500 FYCO1, 1:1000 TSSK2 combined with 1:500 eIF3a , 1:1000 TSSK2 combined with 1:100 eIF3F, 1:1000 TSSK2 alone, 1:500 FYCO1 alone, 1:500 eIF3a alone and 1:100 eIF3f alone diluted in the Duolink antibody diluent. The slides treated with a single antibody and an additional slide with no primary antibody incubation were made to control the performance of the assay. The next day, 2 x 10 min washes with wash buffer A (10 mM Tris, 150 mM NaCl, 0.05% Tween, pH 7.5) were performed before a 60 min incubation with Duolink plus anti-rabbit and minus anti-mouse secondary antibodies. 2 x 10 min wash buffer A washes followed, then a 30 min incubation with Duolink ligation mixture containing 1 ul ligase per sample was performed. Finally, 2 x 10 min buffer A washes were performed prior to 100 min incubation with Duolink amplification mixture containing 0.5 ul polymerase per sample. All of the incubations above were performed at +37 °C in a dark, humified chamber. After the amplification reaction, slides were washed 2 x 15 min with wash buffer B (200 mM Tris, 100 mM NaCl, pH 7.5), 1 min with 0.01x wash buffer B and 2 x 10 min with PBS. 30 min incubation with 1:5000 PNA in PBS and 10 min incubation with 1:10 000 DAPI in PBS followed, then mounting, imaging and image processing similarly to the immunofluorescence slides.

4.5 Translational analysis with L-azidohomoalanine

To investigate the possible connection between the late CB and translation initiation, as hinted by the discovery of eIF3 as a novel TSSK2 interaction candidate, a translational analysis was performed. For this purpose, a non-canonical amino acid analogue, L-azidohomoalanine (AHA) was used to label newly synthesized proteins. First, testes were

collected and decapsulated in methionine free Dulbecco's modified eagle's medium (DMEM, Thermo Fisher Scientific). Seminiferous tubule pieces were cut in stages IX-XII, I-V and VI-VIII according to the light absorption pattern as described earlier in section 2.3.2. of Materials and Methods. The tubule pieces were then transferred to a sterile 96-well plate, with each tubule having one of the following experimental conditions: 300 uM AHA (cat# C10289, Invitrogen, California, USA), 300 uM AHA combined with 50 uM cycloheximide (CHX, cat#C4859, Sigma Aldrich) or DMSO only, all diluted in methionine free DMEM. The conditions with DMSO only and AHA combined with the translation inhibitor CHX were employed to control the performance of the experiment. The incubation was carried out in a +34 °C incubator with CO_2 for 45 min. After the incubation period, the tubule pieces were transferred to a Superfrost Plus glass slide and squashed with a coverslip put on top of them, releasing the germ cells from the tubule. Lens paper was used to absorb excess fluid from the edges of the coverslip, and to spread the cells across the slide. After squashing, the slides were snap frozen in liquid nitrogen to remove the coverslip and fixed in ice cold 96% EtOH for 5 min. The fixed squash slides were then air dried O/N at RT.

The following day, slides were post-fixed 15 min in 4% PFA, washed 2 x 10 min with 3% BSA-PBS, permeabilized 5 min in 0.2% Triton-PBS and washed again 2 x 10 min with 3% BSA-PBS. Next, slides were incubated with 100 uL of the Click-IT reaction mix (Invitrogen) for 30 min at RT, in dark, humified chamber. This induced a click reaction between the azido moiety of AHA and an alkyne moiety of a fluorescent label, with a wavelength of 488 nm. From hereafter, all steps were performed in dark to protect the fluorescent label from photobleaching. One 10 min 3% BSA-PBS wash followed before blocking the slides in 10% BSA for 1 h at RT. Primary incubation with 1:1000 TSSK2 diluted in 3% BSA-PBS was performed O/N at +4 °C. The next day, 3 x 5 min 0.1% Tween-PBS washes were followed by a secondary antibody incubation with 1:500 anti-mouse AlexaFluor 647 and 1:5000 PNA in 3% BSA-PBS for 1 h at RT. Slides were washed 3 x 5 min with 0.1% Tween-PBS, incubated 10 min with 1:10 000 DAPI in PBS, washed one more time with PBS and mounted with Prolong Diamond Antifade with DAPI. Imaging and image processing were done similarly to the immunofluorescence slides.

5. Acknowledgements

Mari Lehti, PhD, Institute of Biomedicine, University of Turku

Noora Kotaja, PhD, Professor, Institute of Biomedicine, University of Turku

6. Abbreviations

AHA l-azidohomoalanine

BSA bovine serum albumin

CB chromatoid body

CHX cycloheximide

DAPI 4′,6-diamidino-2-phenylindole

DDX25 DEAD-box helicase 25

DMEM Dulbecco’s modified eagle’s medium

EDTA ethylenediaminetetraacetic acid

eIF3 eukaryotic initiation factor 3

FYCO1 FYVE and coiled-coil domain containing 1

GAPDH glyceraldehyde 3-phosphate dehydrogenase

GRTH gonadotropin regulated testicular RNA helicase

IgG immunoglobulin

IMC intermitochondrial cement

IP immunoprecipitation

KO knock-out

MILI mouse PIWIL1

miRNA micro RNA

MIWI mouse PIWIL2

MVH mouse VASA homologue

ncRNA non-coding RNA

NDS normal donkey serum

NMD nonsense-mediated RNA decay

PBS phosphate buffered saline

PFA paraformaldehyde

piRNA PIWI-interacting RNA

PLA proximity ligation assay

PMSF phenylmethylsulphonyl fluoride

PNA Rhodamine-conjugated peanut agglutinin

PND postnatal

RNAi RNA interference

RNP ribonucleoprotein

SDS sodium dodecyl sulphate

SDS-PAGE SDS-polyacrylamide gel electrophoresis

SNP single nucleotide polymorphism

TBS Tris-buffered saline

TDRD tudor domain-containing protein

Triton Triton x-100

TSKS testis-specific kinase substrate

TSSK testis-specific serine/threonine kinase

Tween Tween-20/polysorbate 20

WT wildtype

7. References

Agarwal, A., A. Mulgund, A. Hamada, and M.R. Chyatte. 2015. A unique view on male infertility around the globe. *Reprod. Biol. Endocrinol.* 13:37. doi:10.1186/s12958-015-0032-1.

Aizer, A., A. Kalo, P. Kafri, A. Shraga, R. Ben-Yishay, A. Jacob, N. Kinor, and Y. Shav-Tal.

2014. Quantifying mRNA targeting to P-bodies in living human cells reveals their dual role in mRNA decay and storage. *J. Cell Sci.* 127:4443–4456. doi:10.1242/jcs.152975.

Aravin, A.A., G.J. Hannon, and J. Brennecke. The Piwi-piRNA Pathway Provides an Adaptive Defense in the Transposon Arms Race.

Bellve, A.R., J.C. Cavicchia, C.F. Millette, D.A. O'Brien, Y.M. Bhatnagar, and M. Dym. 1977. Spermatogenic cells of the prepuberal mouse. Isolation and morphological characterization. *J. Cell Biol.* 74:68–85. doi:10.1083/jcb.74.1.68.

Chemes, H.E., and C.A. Sedo. 2012. Tales of the Tail and Sperm Head Aches Changing concepts on the prognostic significance of sperm pathologies affecting the head, neck and tail. *Asian J. Androl.* 14:14–23. doi:10.1038/aja.2011.168.

Clermont, Y., and C.P. Leblond. 1955. Spermiogenesis of man, monkey, ram and other mammals as shown by the ?periodic acid-schiff? technique. *Am. J. Anat.* 96:229–253. doi:10.1002/aja.1000960203.

Cocuzza, M., C. Alvarenga, and R. Pagani. 2013. The epidemiology and etiology of azoospermia. *Clinics*. 68:15–26. doi:10.6061/clinics/2013(Sup01)03.

Dai, P., X. Wang, L.T. Gou, Z.T. Li, Z. Wen, Z.G. Chen, M.M. Hua, A. Zhong, L. Wang, H. Su, H. Wan, K. Qian, L. Liao, J. Li, B. Tian, D. Li, X.D. Fu, H.J. Shi, Y. Zhou, and M.F. Liu. 2019. A Translation-Activating Function of MIWI/piRNA during Mouse Spermiogenesis. *Cell*. 179:1566-1581.e16. doi:10.1016/j.cell.2019.11.022.

Deane, J.A., D.G. Cole, E.S. Seeley, D.R. Diener, and J.L. Rosenbaum. 2001. Localization of intraflagellar transport protein IFT52 identifies basal body transitional fibers as the docking site for IFT particles. *Curr. Biol.* 11:1586–1590. doi:10.1016/S0960-9822(01)00484-5.

Fanourgakis, G., M. Lesche, M. Akpinar, A. Dahl, and R. Jessberger. 2016. Chromatoid Body Protein TDRD6 Supports Long 3' UTR Triggered Nonsense Mediated mRNA Decay. *PLoS Genet.* 12. doi:10.1371/journal.pgen.1005857.

Fawcett, D.W., E.M. Eddy, and D.M. Phillips2. 1970. Observations on the Fine Structure and Relationships of the Chromatoid Body in Mammalian Spermatogenesis'. 2. 129–153 pp.

Gatewood, J.M., G.R. Cook, R. Balhorn, E.M. Bradbury, and C.W. Schmid. 1987. Sequence-specific packaging of DNA in human sperm chromatin. *Science (80-.).* 236:962–964. doi:10.1126/science.3576213.

Gustafsdottir, S.M., E. Schallmeiner, S. Fredriksson, M. Gullberg, O. Söderberg, M. Jarvius, J. Jarvius, M. Howell, and U. Landegren. 2005. Proximity ligation assays for sensitive and specific protein analyses. *In* Analytical Biochemistry. Academic Press Inc. 2–9.

Hannon, G.J. 2002. RNA interference. *Nature*. 418:244–251. doi:10.1038/418244a.

Haraguchi, C.M., T. Mabuchi, S. Hirata, T. Shoda, K. Hoshi, K. Akasaki, and S. Yokota. 2005. Chromatoid bodies: Aggresome-like characteristics and degradation sites for organelles of spermiogenic cells. *J. Histochem. Cytochem.* 53:455–465. doi:10.1369/jhc.4A6520.2005.

Hein, C.D., X.M. Liu, and D. Wang. 2008. Click chemistry, a powerful tool for pharmaceutical sciences. *Pharm. Res.* 25:2216–2230. doi:10.1007/s11095-008-9616-1.

Hermo, L., R.M. Pelletier, D.G. Cyr, and C.E. Smith. 2010a. Surfing the wave, cycle, life history, and genes/proteins expressed by testicular germ cells. Part 1: Background to spermatogenesis, spermatogonia, and spermatocytes. *Microsc. Res. Tech.* 73:241–278. doi:10.1002/jemt.20783.

Hermo, L., R.M. Pelletier, D.G. Cyr, and C.E. Smith. 2010b. Surfing the wave, cycle, life history, and genes/proteins expressed by testicular germ cells. Part 3: Developmental changes in spermatid flagellum and cytoplasmic droplet and interaction of sperm with the zona pellucida and egg plasma membrane. *Microsc. Res. Tech.* 73:320–363. doi:10.1002/jemt.20784.

Hermo, L., R.M. Pelletier, D.G. Cyr, and C.E. Smith. 2010c. Surfing the wave, cycle, life history, and genes/proteins expressed by testicular germ cells. part 5: Intercellular junctions and contacts between germs cells and Sertoli cells and their regulatory interactions, testicular cholesterol, and genes/proteins associated with more than one germ cell generation. *Microsc. Res. Tech.* 73:409–494. doi:10.1002/jemt.20786.

Hermo, L., R.M. Pelletier, D.G. Cyr, and C.E. Smith. 2010d. Surfing the wave, cycle, life history, and genes/proteins expressed by testicular germ cells. Part 2: Changes in spermatid organelles associated with development of spermatozoa. *Microsc. Res. Tech.* 73:279–319. doi:10.1002/jemt.20787.

Hinnebusch, A.G. 2006. eIF3: a versatile scaffold for translation initiation complexes. *Trends Biochem. Sci.* 31:553–562. doi:10.1016/j.tibs.2006.08.005.

Ho, H.C., and S. Wey. 2007. Three dimensional rendering of the mitochondrial sheath morphogenesis during mouse spermiogenesis. *Microsc. Res. Tech.* 70:719–723. doi:10.1002/jemt.20457.

Horowitz, E., Z. Zhang, B.H. Jones, S.B. Moss, C. Ho, J.R. Wood, X. Wang, M.D. Sammel, and J.F. Strauss. 2005. Patterns of expression of sperm flagellar genes: early expression of genes encoding axonemal proteins during the spermatogenic cycle and shared features of promoters of genes encoding central apparatus proteins*. *MHR Basic Sci. Reprod. Med.* 11:307–317. doi:10.1093/molehr/gah163.

Jackson, R.J., C.U.T. Hellen, and T. V. Pestova. 2010. The mechanism of eukaryotic translation initiation and principles of its regulation. *Nat. Rev. Mol. Cell Biol.* 11:113–127. doi:10.1038/nrm2838.

Jain, S., J.R. Wheeler, R.W. Walters, A. Agrawal, A. Barsic, and R. Parker. 2016. ATPase-Modulated Stress Granules Contain a Diverse Proteome and Substructure. *Cell*. 164:487–498. doi:10.1016/j.cell.2015.12.038.

Kotaja, N., S.N. Bhattacharyya, L. Jaskiewicz, S. Kimmins, M. Parvinen, W. Filipowicz, and P. Sassone-Corsi. 2006. The chromatoid body of male germ cells: Similarity with processing bodies and presence of Dicer and microRNA pathway components.

Kotaja, N., S. Kimmins, S. Brancorsini, D. Hentsch, J.L. Vonesch, I. Davidson, M. Parvinen, and P. Sassone-Corsi. 2004. Preparation, isolation and characterization of stage-specific spermatogenic cells for cellular and molecular analysis. *Nat. Methods*. 1:249–254. doi:10.1038/nmeth1204-249.

Kueng, P., Z. Nikolova, V. Djonov, A. Hemphill, V. Rohrbach, D. Boehlen, G. Zuercher, A.C. Andres, and A. Ziemiecki. 1997. A novel family of serine/threonine kinases participating in spermiogenesis. *J. Cell Biol.* 139:1851–1859. doi:10.1083/jcb.139.7.1851.

Kwitny, S., A. V Klaus, and G.R. Hunnicutt. 2010. The Annulus of the Mouse Sperm Tail Is Required to Establish a Membrane Diffusion Barrier That Is Engaged During the Late Steps of Spermiogenesis 1. *Biol. Reprod.* 82:669–678. doi:10.1095/biolreprod.109.079566.

Laiho, A., N. Kotaja, A. Gyenesei, and A. Sironen. 2013. Transcriptome Profiling of the Murine Testis during the First Wave of Spermatogenesis. *PLoS One*. 8:e61558. doi:10.1371/journal.pone.0061558.

Lehti, M.S., and A. Sironen. 2016. Formation and function of the manchette and flagellum during spermatogenesis. *Reproduction*. 151:R43–R54. doi:10.1530/REP-15-0310.

Lehtiniemi, T., and N. Kotaja. 2018. Germ granule-mediated RNA regulation in male germ cells. *Reproduction*. 155:R77–R91. doi:10.1530/REP-17-0356.

Li, Y., J. Sosnik, L. Brassard, M. Reese, N.A. Spiridonov, T.C. Bates, G.R. Johnson, J. Anguita, P.E. Visconti, and A.M. Salicioni. 2011. Expression and localization of five members of the testis-specific serine kinase (Tssk) family in mouse and human sperm and testis. *Mol. Hum. Reprod.* 17:42–56. doi:10.1093/molehr/gaq071.

MacLeod, G., P. Shang, G.T. Booth, L.A. Mastropaolo, N. Manafpoursakha, A.W. Vogl, and S. Varmuza. 2014. PPP1CC2 can form a kinase/phosphatase complex with the testis-specific proteins TSSK1 and TSKS in the mouse testis. *Reproduction*. 147:1–12. doi:10.1530/REP-13-0224.

Marchione, R., S.A. Leibovitch, and J.L. Lenormand. 2013. The translational factor eIF3f: The ambivalent eIF3 subunit. *Cell. Mol. Life Sci.* 70:3603–3616. doi:10.1007/s00018-013-1263-y.

Meikar, O., M. Da Ros, H. Korhonen, and N. Kotaja. 2011. Chromatoid body and small RNAs in male germ cells. *Reproduction*. 142:195–209. doi:10.1530/REP-11-0057.

Meikar, O., V. V. Vagin, F. Chalmel, K. Sõstar, A. Lardenois, M. Hammell, Y. Jin, M. Da Ros, K.A. Wasik, J. Toppari, G.J. Hannon, and N. Kotaja. 2014. An atlas of chromatoid body components. *RNA*. 20:483–495. doi:10.1261/rna.043729.113.

Negrutskii, B.S., and A. V. El'skaya. 1998. Eukaryotic Translation Elongation Factor 1α: Structure, Expression, Functions, and Possible Role in Aminoacyl-tRNA Channeling. *In* Progress in Nucleic Acid Research and Molecular Biology. Academic Press. 47–78.

Onohara, Y., and S. Yokota. 2012. Expression of DDX25 in nuage components of mammalian spermatogenic cells: Immunofluorescence and immunoelectron microscopic study. *Histochem. Cell Biol.* 137:37–51. doi:10.1007/s00418-011-0875-2.

Reuter, M., P. Berninger, S. Chuma, H. Shah, M. Hosokawa, C. Funaya, C. Antony, R. Sachidanandam, and R.S. Pillai. 2011. Miwi catalysis is required for piRNA amplification-independent LINE1 transposon silencing. *Nature*. 480:264–267. doi:10.1038/nature10672.

Rocak, S., and P. Linder. 2004. Dead-box proteins: The driving forces behind RNA metabolism. *Nat. Rev. Mol. Cell Biol.* 5:232–241. doi:10.1038/nrm1335.

Da Ros, M., T. Lehtiniemi, O. Olotu, D. Fischer, F.P. Zhang, H. Vihinen, E. Jokitalo, A. Sironen, J. Toppari, and N. Kotaja. 2017. FYCO1 and autophagy control the integrity of the haploid male germ cell-specific RNP granules. *Autophagy*. 13:302–321. doi:10.1080/15548627.2016.1261319.

Russell, L.D., L.E. Alger, and L.G. Nequin. 1987. Hormonal control of pubertal

spermatogenesis. *Endocrinology*. 120:1615–1632. doi:10.1210/endo-120-4-1615.

Russell, L.D., R.A. Ettlin, A.P.S. Hikim, and E.D. Clegg. 1993. Histological and Histopathological Evaluation of the Testis. *Int. J. Androl.* 16:83–83. doi:10.1111/j.1365-2605.1993.tb01156.x.

Russell, L.D., J.A. Russell, G.R. MacGregor, and M.L. Meistrich. 1991. Linkage of manchette microtubules to the nuclear envelope and observations of the role of the manchette in nuclear shaping during spermiogenesis in rodents. *Am. J. Anat.* 192:97–120. doi:10.1002/aja.1001920202.

Salicioni, A.M., M.G. Gervasi, J. Sosnik, D.A. Tourzani, S. Nayyab, D.A. Caraballo, and P.E. Visconti. 2020. Testis-specific serine kinase protein family in male fertility and as targets for non-hormonal male contraception†. *Biol. Reprod.* doi:10.1093/biolre/ioaa064.

Sato, H., C.H. Tsai-Morris, and M.L. Dufau. 2010. Relevance of gonadotropin-regulated testicular RNA helicase (GRTH/DDX25) in the structural integrity of the chromatoid body during spermatogenesis. *Biochim. Biophys. Acta - Mol. Cell Res.* 1803:534–543. doi:10.1016/j.bbamcr.2010.02.004.

Schindelin, J., I. Arganda-Carreras, E. Frise, V. Kaynig, M. Longair, T. Pietzsch, S. Preibisch, C. Rueden, S. Saalfeld, B. Schmid, J.Y. Tinevez, D.J. White, V. Hartenstein, K. Eliceiri, P. Tomancak, and A. Cardona. 2012. Fiji: An open-source platform for biological-image analysis. *Nat. Methods*. 9:676–682. doi:10.1038/nmeth.2019.

Shang, P. 2014. Testis-specific Protein Kinases in Mouse Spermiogenesis. Erasmus University of Rotterdam. Rotterdam, Netherlands. 1–185 pp.

Shang, P., W.M. Baarends, J. Hoogerbrugge, M.P. Ooms, W.A. Van Cappellen, A.A.W. De Jong, G.R. Dohle, H. Van Eenennaam, J.A. Gossen, and J.A. Grootegoed. 2010. Functional transformation of the chromatoid body in mouse spermatids requires testis-specific serine/threonine kinases. *J. Cell Sci.* 123:331–339. doi:10.1242/jcs.059949.

Singh, S., G. Sedgh, and R. Hussain. 2010. Unintended Pregnancy: Worldwide Levels, Trends, and Outcomes. *Stud. Fam. Plann.* 41:241–250. doi:10.1111/j.1728-4465.2010.00250.x.

Sinha, N., S. Pilder, and S. Vijayaraghavan. 2012. Significant Expression Levels of Transgenic PPP1CC2 in Testis and Sperm Are Required to Overcome the Male Infertility Phenotype of Ppp1cc Null Mice. *PLoS One*. 7:47623. doi:10.1371/journal.pone.0047623.

Söderström, K.O., and M. Parvinen. 1976. Transport of material between the nucleus, the chromatoid body and the golgi complex in the early spermatids of the rat. *Cell Tissue Res.* 168:335–342. doi:10.1007/BF00215311.

Sosnik, J., P. V. Miranda, N.A. Spiridonov, S.Y. Yoon, R.A. Fissore, G.R. Johnson, and P.E. Visconti. 2009. Tssk6 is required for Izumo relocalization and gamete fusion in the mouse. *J. Cell Sci.* 122:2741–2749. doi:10.1242/jcs.047225.

Soumillon, M., A. Necsulea, M. Weier, D. Brawand, X. Zhang, H. Gu, P. Barthès, M. Kokkinaki, S. Nef, A. Gnirke, M. Dym, B. deMassy, T.S. Mikkelsen, and H. Kaessmann. 2013. Cellular Source and Mechanisms of High Transcriptome Complexity in the Mammalian Testis. *Cell Rep.* 3:2179–2190. doi:10.1016/j.celrep.2013.05.031.

Tanaka, S.S., Y. Toyooka, R. Akasu, Y. Katoh-Fukui, Y. Nakahara, R. Suzuki, M. Yokoyama, and T. Noce. 2000. The mouse homolog of Drosophila Vasa is required for the development of male germ cells. *Genes Dev.* 14:841–853. doi:10.1101/gad.14.7.841.

Tanaka, T., M. Hosokawa, V. V. Vagin, M. Reuter, E. Hayashi, A.L. Mochizuki, K. Kitamura, H. Yamanaka, G. Kondoh, K. Okawa, S. Kuramochi-Miyagawa, T. Nakano, R. Sachidanandam, G.J. Hannon, R.S. Pillai, N. Nakatsuji, and S. Chuma. 2011. Tudor domain containing 7 (Tdrd7) is essential for dynamic ribonucleoprotein (RNP) remodeling of chromatoid bodies during spermatogenesis. *Proc. Natl. Acad. Sci. U. S. A.* 108:10579–10584. doi:10.1073/pnas.1015447108.

Ubersax, J.A., and J.E. Ferrell. 2007. Mechanisms of specificity in protein phosphorylation. *Nat. Rev. Mol. Cell Biol.* 8:530–541. doi:10.1038/nrm2203.

Unhavaithaya, Y., Y. Hao, E. Beyret, H. Yin, S. Kuramochi-Miyagawa, T. Nakano, and H. Lin. 2009. MILI, a PIWI-interacting RNA-binding protein, is required for germ line stem cell self-renewal and appears to positively regulate translation. *J. Biol. Chem.* 284:6507–6519. doi:10.1074/jbc.M809104200.

Vasileva, A., D. Tiedau, A. Firooznia, T. Müller-Reichert, and R. Jessberger. 2009. Tdrd6 Is Required for Spermiogenesis, Chromatoid Body Architecture, and Regulation of miRNA Expression. *Curr. Biol.* 19:630–639. doi:10.1016/j.cub.2009.02.047.

Voronina, E., G. Seydoux, P. Sassone-Corsi, and I. Nagamori. 2011. RNA granules in germ cells. *Cold Spring Harb. Perspect. Biol.* 3. doi:10.1101/cshperspect.a002774.

Wang, X., Y. Wei, G. Fu, H. Li, H. Saiyin, G. Lin, Z. Wang, S. Chen, and L. Yu. 2014. Tssk4 is essential for maintaining the structural integrity of sperm flagellum. *Mol. Hum. Reprod.* 21:136–145. doi:10.1093/molehr/gau097.

Wei, Y., X. Wang, G. Fu, and L. Yu. 2013. Testis specific serine/threonine kinase 4 (Tssk4) maintains its kinase activity by phosphorylating itself at Thr-197. *Mol. Biol. Rep.* 40:439–447. doi:10.1007/s11033-012-2078-x.

Xu, B., Z. Hao, K.N. Jha, L. Digilio, C. Urekar, Y.H. Kim, S. Pulido, C.J. Flickinger, and J.C. Herr. 2007. Validation of a testis specific serine/threonine kinase [TSSK] family and the substrate of TSSK1 & 2, TSKS, as contraceptive targets. *Soc. Reprod. Fertil. Suppl.* 63:87–101.

Xu, B., Z. Hao, K.N. Jha, Z. Zhang, C. Urekar, L. Digilio, S. Pulido, J.F. Strauss, C.J. Flickinger, and J.C. Herr. 2008a. Targeted deletion of Tssk1 and 2 causes male infertility due to haploinsufficiency. *Dev. Biol.* 319:211–222. doi:10.1016/j.ydbio.2008.03.047.

Xu, B., Z. Hao, K.N. Jha, Z. Zhang, C. Urekar, L. Digilio, S. Pulido, J.F. Strauss, C.J. Flickinger, and J.C. Herr. 2008b. TSKS concentrates in spermatid centrioles during flagellogenesis. *Dev. Biol.* 319:201–210. doi:10.1016/j.ydbio.2008.03.043.

Yabuta, Y., H. Ohta, T. Abe, K. Kurimoto, S. Chuma, and M. Saitou. 2011. TDRD5 is required for retrotransposon silencing, chromatoid body assembly, and spermiogenesis in mice. *J. Cell Biol.* 192:781–795. doi:10.1083/jcb.201009043.

Zhang, K., L. Fu, Q. An, W. Hu, J. Liu, X. Tang, Y. Ding, W. Lu, X. Liang, X. Shang, and Y. Gu. 2020. Effects of Qilin pills on spermatogenesis, reproductive hormones, oxidative stress, and the TSSK2 gene in a rat model of oligoasthenospermia. *BMC Complement. Med. Ther.* 20:42. doi:10.1186/s12906-019-2799-7.

Zhang, Z., X. Shen, B.H. Jones, B. Xu, J.C. Herr, and J.F. Strauss. 2008. Phosphorylation of mouse sperm axoneme central apparatus protein SPAG16L by a testis-specific kinase, TSSK2. *Biol. Reprod.* 79:75–83. doi:10.1095/biolreprod.107.066308.